Drexel University

Annual Progress Report: 2009 Formula Grant

Reporting Period

July 1, 2010 – June 30, 2011

Formula Grant Overview

The Drexel University received $1,431,165 in formula funds for the grant award period January 1, 2010 through December 31, 2012. Accomplishments for the reporting period are described below.

Research Project 1: Project Title and Purpose

Effect of Antiretroviral Therapy on Surrogate Markers of Cardiovascular Disease and Inflammation in HIV-infected Patients - Numerous studies have demonstrated that HIV infected patients are at an increased risk of developing cardiovascular disease (CVD) and myocardial infarction (MI). There is evidence to suggest that HIV infected patients have unique risk factors related to their infection and its treatment that interact with traditional cardiac risk factors to put them at increased risk of CVD. The purpose of this study is to prospectively evaluate measures of endothelial function and subclinical atherosclerosis as well as markers of inflammation in HIV patients in order to elucidate the nature of HIV specific risk factors for cardiovascular disease. This knowledge will allow more effective risk stratification and treatment in this population which is disproportionally affected by cardiovascular disease.

Anticipated Duration of Project

1/1/2010 - 12/31/2012

Project Overview

We will conduct a prospective cohort study examining the affect of initiating anti-retroviral therapy (ART) on structural, immunologic, and functional markers of atherosclerosis. We hypothesize that although some components of ART may carry increased risk of CVD, the net effect of viral suppression will be decreased inflammation with resultant decreased atherogenesis and improved endothelial function. Our study will address the following specific aims:

Specific Aim 1: To determine if HIV infection is associated with increased inflammation decreased endothelial function, and increased risk for atherosclerosis.
Specific Aim 2: To determine if initiation of ART in HIV infected adults is associated with improvement of markers of inflammation, endothelial function and atherosclerosis.
Specific Aim 3: To assess for correlation between changes in immune activation and changes in markers of inflammation and subclinical atherosclerosis.

We will accomplish these aims by conducting a prospective observational cohort study focusing on 3 groups: HIV infected subjects who initiate ART, HIV infected subjects who do not initiate ART, and HIV negative subjects with the following specific objectives: 1) To compare mean change at one year in carotid artery intima-media thickness (IMT) between the three study groups. 2) To compare changes in inflammatory markers, brachial artery Flow Mediated Dilation (FMD), cardiac ejection fraction and pulmonary artery pressure at one year between the three study groups. 3) To assess for correlation between changes in serum markers of inflammation, status of HIV disease (as measured by CD4 and viral load), endothelial activation, physiologic surrogates of CVD such as IMT and FMD and cardiac function.

Principal Investigator

Christopher J. Bruno, MD
Assistant Professor of Medicine
Drexel University College of Medicine
245 N. 15th Street
Mail Stop 461
Philadelphia, PA 19102

Other Participating Researchers

Jeffrey Jacobson, MD, Howard Eisen, MD, Andrew Kohut, MD, Michele Kutzler, PhD – employed by Drexel University College of Medicine

Expected Research Outcomes and Benefits

As HIV-infected patients live longer, the recognition and treatment of other chronic illnesses have taken on increased significance in this population. Cardiovascular disease (CVD) is of particular importance since several large cohort studies have demonstrated an increased prevalence of CVD, and a higher risk for myocardial infarction (MI) in HIV-infected patients in the ART era.

This study will collect preliminary data that will allow us to begin to correlate observations from the clinical realm with changes at the molecular level to better understand the mechanisms of atherosclerotic disease in HIV infected patients. Measurement of circulating markers of immune and endothelial activation will provide an insight into the pathophysiology of CVD at the molecular level. Structural and functional measurements of atherosclerosis will provide a macroscopic correlate. We expect that through this approach we will gain a better understanding of the pathophysiology of this process with the long term goal of establishing biomarkers of CVD in HIV infected patients that can be used in combination with clinical data to predict and monitor CVD in HIV patients in clinical care.

Summary of Research Completed

During this funding period, we enrolled 10 patients. Subjects were enrolled from one of 2 sites: the Drexel University College of Medicine Partnership Comprehensive Care Practice for HIV

positive subjects, and the General Medicine Clinic at 1427 Vine Street for HIV uninfected subjects. Study related tests were conducted at the Partnership or Hahnemann University Hospital, both located in center city Philadelphia.

Inclusion Criteria: HIV Positive Subjects
Patients were eligible for enrollment in this study if they: 1) Have HIV infection as documented by a clinically licensed ELISA test and confirmed by Western Blot testing 2) Are eighteen years or older 3) Are not currently on ART and have not been on ART within the last one year and 4) Are free of exclusion criteria as listed below.

Inclusion Criteria: HIV Negative Subjects
Patients from the general medical clinic were eligible for enrollment if they were 1) Eighteen years or older 2) Are documented to be HIV negative by a clinically licensed ELISA test and 3) Are free from the exclusion criteria as listed below.

Exclusion Criteria: Both HIV Positive and HIV Negative Subjects
Patients were ineligible to participate in the study if they met any of the following criteria: History of coronary artery disease including: prior history of myocardial infarction, coronary artery bypass surgery, angioplasty or angina pectoris with a stress test or coronary angiography indicating coronary artery disease. History of stroke, transient ischemic attack, or documented carotid atherosclerosis; use of lipid lowering medications within six months prior to study entry. Pregnant at time of screening or plans to become pregnant during the study period.
Any diagnosis of diabetes mellitus, with the exception of a previous history of gestational or steroid-induced diabetes mellitus within 12 weeks prior to study entry. Current use of immunosuppressive medications including current use of systemic steroids (IV or PO), immunosuppressive regimens for solid organ or stem cell transplantation, TNF-alpha antagonists, or monoclonal antibody therapy. Chronic active hepatitis B or C infection. History of chemotherapy within the six months prior to study enrollment. History of active autoimmune disease including SLE, rheumatoid arthritis, sarcoidosis, multiple sclerosis, myasthenia gravis. Diagnosis of active tuberculosis or currently undergoing treatment for active tuberculosis. Active drug or alcohol use or dependence that, in the opinion of the site investigator, would interfere with adherence to study requirements. Impaired mental status that in the opinion of the site investigator precludes the possibility of informed consent.

Subjects were identified by their provider or by self referral from posted advertising in participating clinics. Patients interested in participating in the study were scheduled to meet with a member of the study team for a screening visit. At this visit the subject was provided with more information about the details of study requirements and was consented for study participation. Subjects in the treatment group initiated ART within one month of their screening visit.
Study enrollment will continue until the designated sample size is reached. Subject's active participation in the study will last 48 weeks. The study will be concluded when the last enrolled subject has reached week 48. Data analysis is expected to be completed within 6 months of study completion.

Research Project 2: Project Title and Purpose

Modulation of Capsid Stability as an Antiviral Strategy - The project purpose is to identify anti-HIV compounds that work by antagonizing the functions of the viral capsid protein.

Duration of Project

1/1/2010 - 6/30/2011

Project Overview

The HIV-1 capsid (CA) is an essential viral protein that performs two major roles in the life cycle of HIV-1: one structural, in which it forms a protein shell that shields both the viral genome and the replicative enzymes of HIV-1, and the other regulatory, in which the precise temporal disassembly of this shell coordinates post-entry events such as reverse transcription. The CA protein is composed of two domains: the C-terminal domain (CTD) and the N-terminal domain (NTD). Both of these domains make critical inter- and intradomain interactions that are critical for the formation of the capsid shell. Recently, the atomic structure of the hexameric building block of the HIV-1 capsid shell has been determined. This structure offers new insights into the molecular details of the hexameric assembly of CA, in particular revealing features of the NTD-NTD interface that may be exploited therapeutically.

The NTD of the capsid protein is the structural anchor for the formation of the hexameric lattice by which the HIV-1 capsid assembles. The stability of this hexameric lattice, which is also conferred by the NTD, regulates the precise temporal series of replicative events after fusion; capsids that are too stable or too unstable do not enter into reverse transcription correctly. Therefore, in theory, any compound that disrupts the normal interactions of the capsid—whether by inhibiting assembly, accelerating disassembly, or artificially stabilizing the core—should attenuate or even kill the virus. The essential roles played by capsid within the HIV-1 life cycle, coupled with the existence of known compounds with the ability to disrupt CA-CA interactions, make the capsid's hexamerization interface a new, attractive therapeutic target.

We therefore propose to identify and characterize the properties of novel small molecules that bind at the NTD-NTD interface. This will be achieved using the newly available structure of the hexameric HIV-1 capsid lattice in conjunction with the novel hybrid structure–based (HSB) in silico screening protocol. Small-molecule "hexamerization antagonists or agonists" identified by this process would represent a new class of capsid inhibitor, targeted at a highly conserved oligomerization surface and possessing a novel mechanism of action. A cross-disciplinary approach comprised of computational, virologic, chemical, and biochemical assays will then be employed to validate, understand, and augment such inhibitors. We believe that this strategy will successfully identify pharmacologically useful reagents that can be used to gain insight into the biological functions of HIV-1 CA protein, such as uncoating and assembly. In addition, small molecules identified from this study hold promise as lead compounds for a new class of antiviral agent.

Principal Investigator

Simon Cocklin, PhD
Research Assistant Professor
Drexel University College of Medicine
Room 10308-312
Department of Biochemistry & Molecular Biology
245 North 15th Street
Philadelphia, PA 19102

Other Participating Researchers

Sandhya Kortagere, PhD - employed by Drexel University College of Medicine
Joseph G. Sodroski, MD - employed by Dana-Farber/Harvard Cancer Center
Wesley Sundquist - employed by University of Utah
Amos B. Smith, III - employed by University of Pennsylvania

Expected Research Outcomes and Benefits

Acquired immune deficiency syndrome (AIDS), caused by the human immunodeficiency virus (HIV-1), is a global epidemic that comprises one of the world's major health problems. Currently, over 40 million people are infected with HIV-1, leading to 3 million deaths from AIDS or AIDS-related causes every year. Despite recent progress in anti-HIV therapy, drug toxicity and the emergence of drug-resistant isolates during long-term treatment of HIV-infected patients necessitate the search for new targets that can be used to develop novel antiviral agents. It is very unlikely that any single inhibitor will be the sole solution to these problems. The more stages of the viral life cycle that can be antagonized, however, the more likely it is that the virus would be forced to mutate at the expense of its fitness, and the less likely that enough viral replication would occur to generate escape mutants. Given the essential roles, both structural and regulatory, of capsid within the HIV-1 life cycle, and the existence of compounds with the ability to disrupt CA-CA interactions, the capsid comprises a tractable therapeutic target. In this project we will identify, characterize, and augment novel small molecules designed to bind the capsid and antagonize its function. These "capsid hexamerization antagonists or agonists" would represent a new class of small-molecule capsid inhibitors, targeted at a highly conserved oligomerization surface and possessing a novel mechanism of action. We believe these data will not only provide new reagents for the dissection of the basic biology of HIV-1 replication and pathogenesis, but will also lay the foundation for a major new initiative in HIV-1 drug discovery.

Summary of Research Completed

Size reduction and optimization of CK026: identification of I-XW-053. As compound CK026 displayed activity in single- and multiple-round infection assays using cell lines, we reasoned that the compound may be poorly permeable across the PBMC membrane. This is probably a function of its poor drug-like properties (high octanol water partition coefficient [logP] of 9.31 as determined using the weighted logP function in Jchem; ChemAxon, Budapest, Hungary) and large molecular weight (692 Da). As such, we sought to reduce the size of the compound and

optimize its physical-chemical properties and to improve its permeability while retaining its antiviral activity. CK026 has C2 symmetry along the central dibenzofuran ring. Docking results suggested that the proposed binding area of CK026 spans the entire NTD dimer interface including the junction between the N- and C-terminal lobes (Figure 2). Based on the docking model, the upper arm of CK026 is proposed to interact with residues Arg173, Asp166, Lys170, Tyr169, Glu180, Gln179, Ser33, and Pro34 and the lower arm with Pro38, Met39, Glu35, Lys30, and Val36. Owing to its symmetry, docking solutions indicated that either arm could occupy either of the two sites; there was no preference for one arm over the other. In order to test these docking observations, two analogues of CK026 were designed. The first, I-XW-091, is composed of the furan ring linker region attached to one arm of the parental molecule whereas the other, I-XW-053, corresponded to only the arm structure. In addition, the benzoic acid moiety on CK026 was predicted from the docking pose to form hydrogen bond interactions with Gln179 and Glu180 of CA. We therefore tested this prediction, and how critical these potential interactions were to the antiviral activity of CK026, by synthesizing DMJ-I-073, a dimethyl ester variant of CK026, which removed the hydrogen-bonding capability at this region. These compounds were then subjected to antiviral analysis using the single-round infection assay. As can be seen in Figure 1, DMJ-I-073 lost all activity in the single-round infection assay, indicating that potential hydrogen bonds formed by benzoic acid moiety in CK026 are key to its activity. Compounds I-XW-053 and I-XW-091, however, retained the activity of the parental molecule, reducing the replication of both YU-2 and AMLV (data not shown) pseudotyped viral particles. I-XW-091 could not be tested at lower concentrations due to its poor solubility in DMSO I-XW-053, which retains the antiviral activity of CK026, represents a significant reduction in molecular size (692 vs 340 Da) and improvement in physical-chemical properties (logP 9.31 vs 5.05), so we therefore decided to test I-XW-053 in the PBMC assay. I-XW-053 has an IC_{50} value for inhibition of the HIV-$1_{92BR030}$ isolate replicating in primary PBMCs comparable to that exhibited by the parental CK026 against HIV-1_{IIIB} replicating in P4-R5 MAGI cells.

I-XW-053 binds to HIV-1 CA and stops its assembly in vitro. Compound I-XW-053 is predicted to interact with the NTD of HIV-1 CA and thereby alter its assembly. However, it is possible that the compound exerts its action via another mechanism not involving CA. We therefore wished to establish that I-XW-053 is directed against HIV-1 CA. The direct interaction of I-XW-053 was assayed using SPR interaction analyses. Wild-type HIV-1 CA protein was purified as outlined in "Materials and methods" and immobilized onto the surface of a high-capacity CM7 sensorchip. A surface to which the monoclonal antibody 17b (a generous gift from Dr. James E. Robinson, Department of Pediatrics, Tulane University Medical Center, New Orleans, LA) was immobilized was used to correct for background binding and instrument and buffer artifacts. I-XW-053 directly interacts with sensorchip-immobilized HIV-1 CA (Figure 2A)**.** In contrast, the small-molecule CD4 mimetic compound NBD-556 displayed no such interaction with HIV-1 CA, establishing the specificity of I-XW-053 for HIV-1 CA (Figure 2B). Interestingly, fitting of the SPR data indicated that the I-XW-053 interacted with HIV-1 CA with a 2:1 stoichiometry.

The binding of I-XW-053 to HIV-1 CA was further characterized thermodynamically by ITC. Figure 3A shows the calorimetric titration of HIV-1_{NL4-3} CA with I-XW-053 at 25°C in Tris-HCl, 150 mM NaCl with 3% DMSO (the exact buffer used for the SPR experiment). The experimental data fitted to a binding model wherein two molecules of I-XW-053 bind to one CA molecule with equal affinity, supporting the 2:1 stoichiometry obtained from SPR analysis. The

affinity of the I-XW-053–CA interaction at 25°C was determined to be 85 µM, corresponding to a change in Gibbs energy of -6.6 kcal/mol per mole of I-XW-053. The changes in enthalpy (ΔH) and entropy (ΔS) were -7.3 kcal/mol and -5.0 cal/(K × mol), respectively, and the change in heat capacity, calculated from temperature dependence of the enthalpy, was -220 cal/(K × mol) (Figure 3B). As such, the measured thermodynamic parameters are typical for the binding of a small molecule that binds without inducing any major conformational changes in the target protein.

I-XW-053 is a specific inhibitor of HIV-1 replication. We next sought to define the antiviral spectrum of I-XW-053. To achieve this, I-XW-053 was evaluated in CPE assays against a panel of viruses from different classes (data not shown). I-XW-053 was evaluated against this panel of viruses up to a highest concentration of 100 µM. The compound displayed no inhibitory effects on the replication of Dengue serotypes 1-4, influenza H1N1, respiratory syncytial virus, yellow fever, Japanese encephalitis, Vaccinia, or Chikungunya viruses. Therefore, I-XW-053 appears to be specific for HIV-1, while further experiments are needed to confirm the null activity against other retroviruses.

I-XW-053 displays broad antiviral activity against multiple subtypes of HIV-1. A key issue in the development of novel HIV drugs is their ability to inhibit the replication of genetically diverse isolates, especially isolates from the most globally prevalent subtypes (A, B, and C). Therefore, the antiviral efficacy of I-XW-053 was evaluated in a standardized PBMC-based anti-HIV-1 assay with a panel of HIV-1 clinical isolates and laboratory strains from different geographic locations that included HIV-1 group M subtypes A, B, C, D, E , F, and G, as well as HIV-1 group O (Table 1). The panel included CCR5-tropic (R5), CXCR4-tropic (X4), and dual-tropic (R5X4) viruses. I-XW-053 inhibited the replication of viruses from all group M subtypes (A, B, C, D, E, F, and G) and also the group O isolate with IC50 values in the range 9-100 µM.

Publications, Posters, Abstracts from This Study

Manuscripts

Kortagere, S., Madani, N., Mankowski, M.K., Schön, A., Princiotto, A., Anthony, K., Zentner, I., Oza, A., Sierra, L.J., Passic., S.R., Wang, X., Jones, D., Carter, J., Stavale, E., Krebs, F.C., Martín-García, J., Freire, E., Ptak, R.G., Sodroski, J., Cocklin, S.,* and Smith, A.B. III* Inhibiting Early-Stage Events in HIV-1 Replication by Small-Molecule targeting of the HIV-1 Capsid. *Journal of Virology*. Submitted, currently being modified as per reviewers recommendations. *corresponding authors

Abstracts/Posters presented

Sandhya Kortagere, Navid Madani, Marie K. Mankowski, Amy Princiotto, Kevin Anthony, Luz-Jeannette Sierra, Xiaozhao Wang, David Jones, Joel R. Courter, Eric Stavale, Roger Ptak, Amos B. Smith, III, Julio Martín-García, Joseph Sodroski, and Simon Cocklin. *Small-molecule HIV-1 capsid inhibitor design using hybrid structure based methods.* 55th Annual Meeting of the Biophysical Society, Baltimore, MD (March 5-9, 2011).

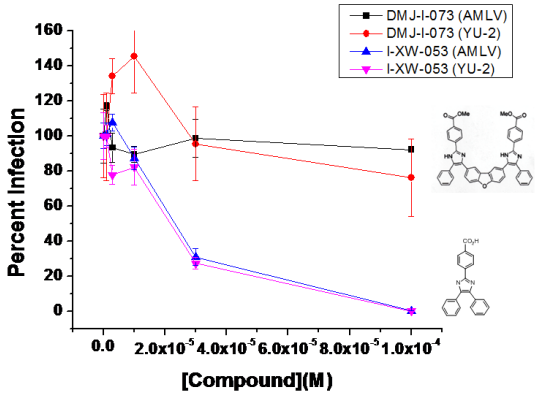

Figure 1. The effect of compounds DMJ-I-073 and I-XW-053 on viral replication. Shown are the effects of compounds DMJ-I-073 and I-XW-053 on the infection of Cf2Th-CCR5 cells by recombinant luciferase-expressing HIV-1 bearing the envelope glycoprotein of the HIV-1_{YU-2} strain or AMLV. Virus infection is expressed as the percentage of infection (measured by luciferase activity in the target cells) observed in the presence of the compound relative to the level of infection observed in the absence of the compound. The data from 3 replicates are shown. IC_{50} for compound I-XW-053 against HIV-1 is 22.5 ± 1.1 µM. The chemical structures of compounds DMJ-I-073 and I-XW-053 are shown in the insets and next to their corresponding dose curves.

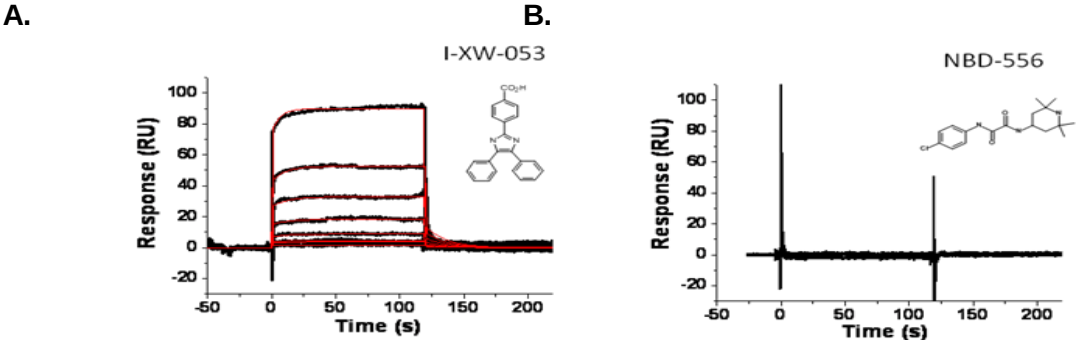

Figure 2. SPR direct binding data for compounds (A) I-XW-053 and (B) NBD-556 to sensor chip-immobilized wild-type HIV-1$_{NL4-3}$ CA. SPR analysis was performed on a CM7 high-capacity sensor chip with a high density of surface immobilized CA protein (7000 RU). Compounds in the concentration range 0.84–110 µM were analyzed. A surface to which the monoclonal antibody 17b had been immobilized served as reference. The small-molecule CD4 mimetic NBD-556 served as a small-molecule control. Black lines indicate experimental data, whereas red lines indicate fitting to a 1:1 Langmuir binding model. The K_D for the interaction of I-XW-053 with HIV-1 CA was found to be 39.3 ± 4.8 µM.

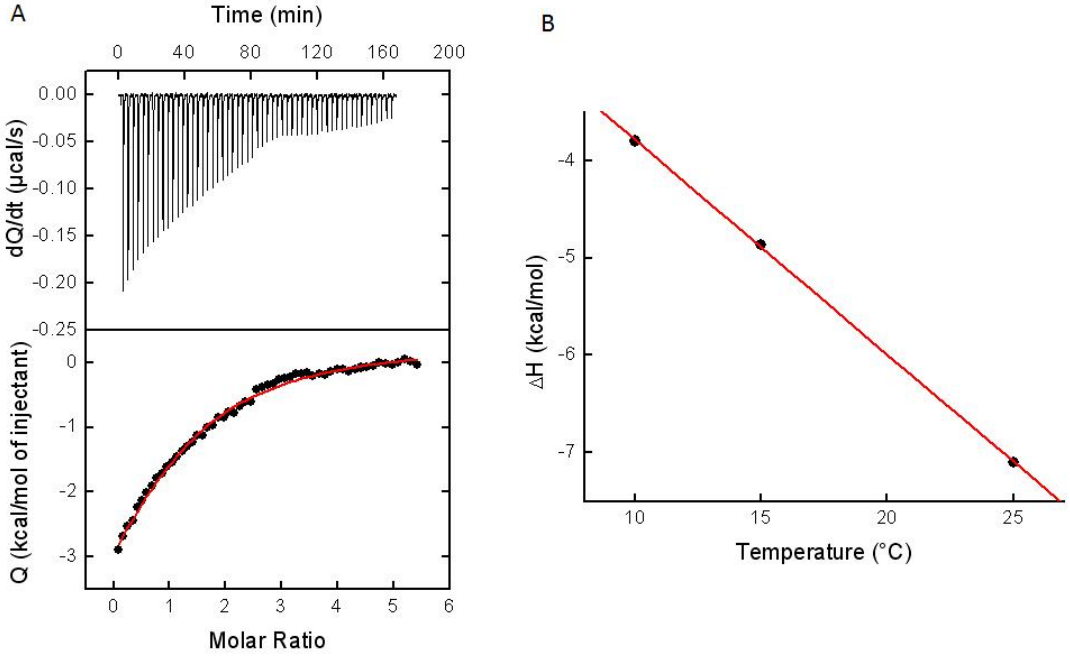

Figure 3. (A) Calorimetric titration of HIV-1$_{NL4-3}$ CA with I-XW-053 at 25°C in Tris-HCl, 150 mM NaCl with 3% DMSO. The concentration of CA was 35 µM, and the syringe contained I-XW-053 at a concentration of 600 µM. The experimental data fit with a binding model whereby two molecules of I-XW-053 bind to one CA, each with a binding affinity of 85 µM, which corresponds to a change in Gibbs energy of -6.6 kcal/mol. The changes in enthalpy (ΔH) and entropy (ΔS) are -7.3 kcal/mol and -5.0 cal/(K × mol), respectively. *(B) Temperature dependence of the enthalpy of binding of I-XW-053 to CA.* The slope corresponds to a heat capacity change of -220 cal/(K × mol).

Table 1. Therapeutic spectrum of I-XW-053.

Virus strain*	IC_{50} (μM)	TC_{50} (μM)	Antiviral index (TC_{50}/IC_{50})
92UG031	93.6	>100	> 1.07
89BZ167	92.9		> 1.08
92BR030	68.7		>1.46
92BR025	51.0		>1.96
93IN101	48.4		>2.07
92UG024	51.8		>1.93
CMU08	100		>1
93BR020	65.6		>1.53
G3	9.03		>11.1
BCF02	71.3		>1.4

*92UG031 = HIV-1 subtype A clinical isolate; 89BZ167 = HIV-1 subtype B clinical isolate; 92BR030 = HIV-1 subtype B clinical isolate; 92BR025 = HIV-1 subtype C clinical isolate; 93IN101 = HIV-1 subtype C clinical isolate; 92UG024 = HIV-1 subtype D clinical isolate; CMU08 = HIV-1 subtype E clinical isolate; 93BR020 = HIV-1 subtype F clinical isolate; G3 = HIV-1 subtype G clinical isolate; BCF02 = HIV-1 group O clinical isolate.

Research Project 3: Project Title and Purpose

sPLA2 Inhibition Therapy for Epilepsy - This project will test the efficacy of new secreted phospholipase A2 (sPLA2) inhibitors as therapy for both the excitability disturbances and inflammatory consequences of epilepsy. These inhibitors, called CHECs, consist of 7mer and 9mer peptides with demonstrated systemic efficacy in traumatic and autoimmune disease models. They are part of a portfolio of intellectual property (composition of matter, applications, diagnostic) held by Drexel University. The goal of this application is to expedite the clinical development of these peptides by expanding potential clinical applications. These compounds are especially suited for commercial development since it has been unequivocally demonstrated that they are active when taken by mouth. The present experiments are proof-of-concept studies for treatment of epilepsy, where the inflammatory consequences of the disease have been largely overlooked. Interestingly, there is also evidence, including our own preliminary studies, that excitability changes during epilepsy are closely related to inflammation, raising the possibility that the CHEC peptides represent a unique monotherapy for this disease.

Anticipated Duration of Project

1/1/2010 - 12/31/2012

Project Overview

SPECIFIC AIM 1 - Inflammation, sPLA2 inhibition and seizure control.
We will screen two systemically active peptide inhibitors of sPLA2 enzymes CHEC-7 and CHEC-9 in a kainic acid seizure model applied to early postnatal and young adult rats. A wealth of data exists that demonstrates the anti-inflammatory and survival promoting activity of these compounds, and preliminarily, their influence of excitability and synaptic functions. We will now apply these peptides to the KA model to explore both contribution and consequences of sPLA2 enzyme activity in seizure disorders. We will measure the following in P13-16 and P35-40 KA models:
a. Motor seizure activity, including potential critical periods for effective sPLA2 inhibition.
b. The time course of changes in enzyme activity, lipid products and substrates (many of the latter are potent inflammatory mediators) using assays specific for sPLA2s, 2D TLC, and mass spectroscopy. These measurements include systemic activity (plasma, urine), and the activity found in the soluble and synaptosomal fractions of cerebral cortex (including hippocampus).

SPECIFIC AIM 2. Inflammatory correlates of childhood and adolescent/young adult epilepsy.
It is our hypothesis that the period of sPLA2 elevation (relative to stable patients) represents the period of maximum vulnerability to seizure-induced inflammatory destruction of central nervous system (CNS) tissue, presumably instigated by inflammatory mediators and the cellular participants in the immune response. We therefore will measure plasma and urinary sPLA2 activity and levels of selected phospholipids in young epileptic patients and compare to seizure history. The relationship of systemic inflammation to other epidemiological and clinical parameters such as age, duration of epilepsy, type of epilepsy and medication will also be determined.

Principal Investigator

Timothy Cunningham, PhD
Professor
Drexel University College of Medicine
2900 Queen Lane
Philadelphia, PA 19129

Other Participating Researchers

Agustin Legido, MD, PhD, MBA, Ignacio Valencia, MD, Divya Subramanian-Khurana, MD – employed by Drexel University College of Medicine

Expected Research Outcomes and Benefits

These experiments are proof-of-concept studies for treatment of epilepsy, where the inflammatory consequences of the disease have been largely overlooked. Interestingly, there is also evidence, including our own preliminary studies, that excitability changes during epilepsy are closely related to inflammation, raising the possibility that the CHEC peptides, that are the subject of this research, represent a unique monotherapy for this disease.

Seizures in humans produce high levels of sPLA2 making these enzymes a worthwhile therapeutic target for controlling hyperexcitability and subsequent inflammatory pathology. The CHEC peptides, which are sPLA2 inhibitors, are ideally suited for this therapy, since they are effective orally and operate on an "as needed" basis.

Summary of Research Completed

We have continued to confirm the efficacy of the CHEC inhibitors of sPLA2 activity in the Kainic acide epilepsy model. This has led to several dramatic displays of acute seizure inhibition and we have documented the time course and extent of inhibition by video recording. The rats shown in the still shot from the video "A" are typical of our results. In this case the rats were simultaneously injected with kainic acid (1.5 mg/kg) and CHEC-9 or vehicle. Note the seizure is stereotypical for kainic acid as for other excitotoxins: beginning with nodding and automatation of the mouth, spreading unilaterally to one limb, rearing and involvement of both limbs, followed by a loss of balance. The seizure is completely inhibited after sPLA2 inhibition with the CHEC peptides. Partial or complete inhibition by CHEC peptides was demonstrated in 14/18 rats while only 4 vehicle treated rats failed to show seizure activity after kainic acid treatment.

The second half of the study is still in progress. This involves measurement of systemic sPLA2 activity post seizure in children and young adults. So far the number of sample collected in insufficient to make meaningful conclusions, according to pre-study predictions of sample size by power analysis. The purpose of these studies is to begin to investigate the contribution of sPLA2 activity to seizure activity in humans, initially by a simple correlative study.

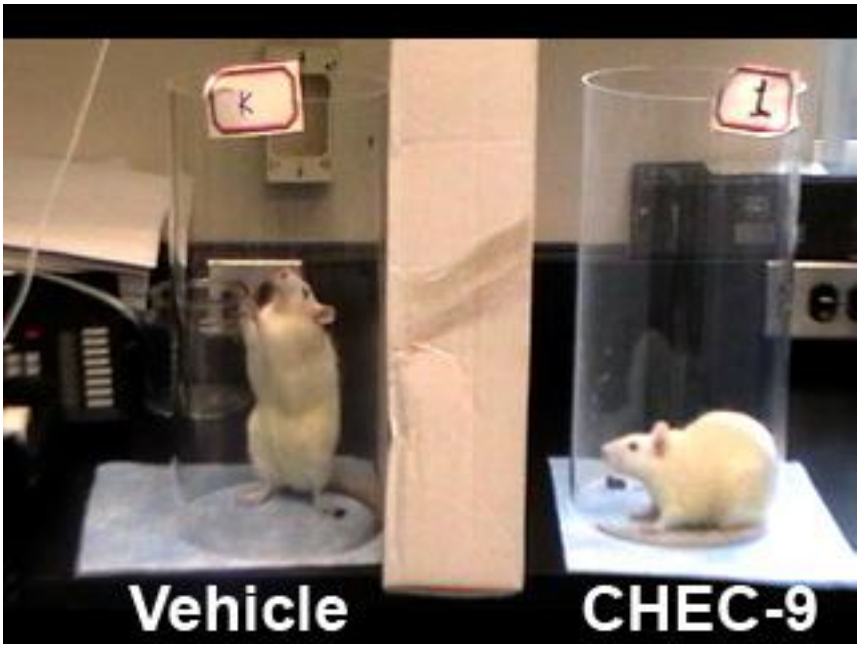

Research Project 4: Project Title and Purpose

Role of Septins in Growth Cone Guidance - This project will investigate the roles of three members of the septin family of GTPase (septin 2,6,7) in the guidance of growth cones by extracellular signaling molecules. The correct guidance of axons is crucial to nervous system development and regeneration following injury. The project will determine if septins are involved in growth cone guidance and the extension of axons, and thus whether they may be targets for therapeutics aimed at promoting or regulating axon extension and regeneration.

Duration of Project

1/1/2010 - 6/30/2011

Project Overview

The broad objective of the project is to determine if septin 6 and 7 are involved in growth cone guidance using in vitro model systems and in vivo analysis of growth cone guidance. The project has two main aims: (1) Analysis of the spatiotemporal dynamics of septins during guidance, and (2) Elucidation of the functions of septin 6 and 7 in axon extension and guidance.

Principal Investigator

Gianluca Gallo, PhD
Associate Professor
Drexel University College of Medicine
2900 Queen Lane
Philadelphia, PA 19129

Other Participating Researchers

Elias Spiliotis, PhD – employed by Drexel University

Expected Research Outcomes and Benefits

The extension and guidance of axons is a fundamental aspect of the regeneration of neuronal connections following injury. A comprehensive understanding of the mechanisms of extension and guidance will provide a platform for the design of therapeutic interventions aimed at promoting regeneration or the targeting of axons following injury. This project will determine whether septin family members may be targeted to promote the extension and/or guidance of axons.

Summary of Research Completed

The main hypothesis of this proposal is that the actin and microtubule cytoskeleton is regulated by SEPT6 and SEPT7 during axon morphogenesis and guidance. We have shown that SEPT6 and SEPT7 localize to portions of filopodia in growth cones and along the axon shaft. SEPT6,

but not SEPT7, promotes the formation of filopodia, and septins regulate growth cone dynamics and size. In order to gain additional insights into how septins might regulate the neuronal cytoskeleton we have now investigated the roles of these septins in the actin and microtubule cytoskeleton of embryonic chicken sensory axons.

Axon collateral branches are initiated by the formation of axonal filopodia and filopodia that become invaded by microtubules can mature into branches. Axonal filopodia in turn arise from precursor actin patches, which arise spontaneously along the axon and have finite durations. Only a subset of patches normally gives rise to filopodia. The mechanism of collateral branching shares similarities to growth cone guidance. In both cases microtubule targeting to filopodia is the initiating event. Moreover, the homogeneity of axonal filopodia provides a reliable platform for analysis of the role of septins in microtubule targeting to filopodia.

In this period we focused our analysis on the role of septins 6 and 7 in formation of axonal filopodia and collateral branches. We found that overexpression of SEPT6 and SEPT7, and respectively shRNA-mediated depletion of these septins, increases and decreases the formation of axonal collateral branches (Figure 1). We also found that treatment with FCF, a pharmacological inhibitor of septin filament turnover that copies the effects of overexpression, increased the formation of axon collateral branches (not shown; $p<0.001$).

Through immunocytochemistry we found that SEPT6 targets to axonal actin patches that serve as precursors to the formation of filopodia, while SEPT7 targets to the base of established filopodia but minimally to actin patches (previously shown). Double labeling studies suggest that SEPT6 and SEPT7 exhibit some overlap at the base of filopodia (not shown; further discussed below). We now performed live imaging of GFP-SEPT7 in conjunction with phase contrast imaging of filopodial formation and we found that SEPT7 accumulates at the base of the filopodium soon after filopodial emergence (Figure 2). We found that overexpression of SEPT7 and shRNA-mediated depletion of SEPT7 increase and decrease, respectively, the percentage of axonal filopodia that contain microtubules (Figure 3). Overexpression of SEPT7 also resulted in increased numbers of actively polymerizing microtubule tips, as revealed by EB1 staining (Figure 3). Furthermore, overexpression of SEPT7, but not SEPT6, also increased the frequency of localized debundling of axonal microtubules and the debundling correlated with local accumulation of SEPT7 (Figure 3), as revealed by immunofluorescence and platinum replica electron microscopy (collaborative work with Dr. T. Svitkina, University of Pennsylvania). Overexpression of SEPT6 did not affect microtubule targeting to axonal filopodia. However, shRNA-mediated depletion decreased the targeting of microtubules to filopodia, suggesting a required but not instructive role for SEPT6 in targeting microtubules to filopodia. Biochemical analysis (not shown) of the physical association of SEPT6 and SEPT7 through immuno-precipitation revealed that a proportion of SEPT6 and SEPT7 are found in a complex, as predicted by the SEPT2-SEPT6-SEPT7 oligomer model. Thus some SEPT6 may contribute to the function of SEPT7 as an obligate oligomerization partner in the role of SEPT7 in the regulation of the targeting of axonal microtubules to filopodia.

SEPT6 in contrast localizes to the axonal actin patches that serve as precursors to the formation of axonal filopodia and is found in a punctate distribution throughout filopodia, both along the axon and at the growth cone. Live imaging of GFP-SEPT6 andphase contrast or mCherry-actin

detailed that SEPT6 is recruited to the base of filopodia and patches early on in their development and persists throughout the duration of patches (Figure 2C). Overexpression of SEPT6 and shRNA-mediated depletion selectively increased and decreased, respectively, the probability that an actin patch will give rise to a filopodium (Figure 4). Manipulation of SEPT7 and SEPT6 had no effect on rate of formation of axonal actin patches, or the lifespan of actin patches. Collectively, these data unveil for the first time septin specific roles in the regulation of the neuronal cytoskeleton. SEPT6 is found to promote the formation of filopodia while SEPT7 promotes the entry of axonal microtubules into filopodia and the splaying of axonal microtubules. Collectively, these actions of SEPT6 and SEPT7 promote the formation of axon collateral branches and based on the similarity in the distribution of SEPT6 and SEPT7 in filopodia and the growth cone and along the axon shaft suggest similar roles of septins during guidance. A manuscript detailing our work on the functions of SEPT6 and SEPT7 in regulating the axonal cytoskeleton is currently in review.

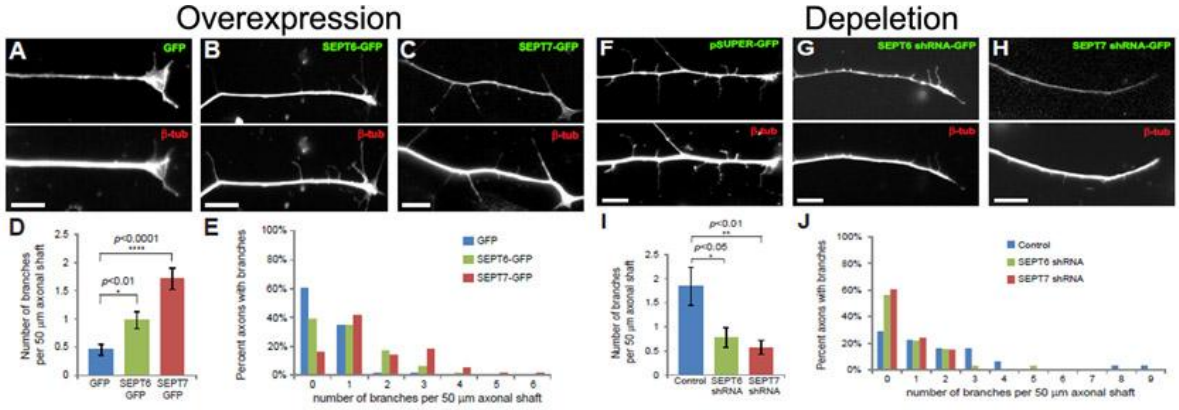

Figure 1. (A-C) examples of axonal morphology in neurons overexpressing SEPT6 or SEPT7. (D-E) quantification of axon branching in overexpression experiments. (F-H) examples of axonal morphology in neurons expressing shRNA against SEPT6 and SEPT7. (I-J) quantification of axon branching in depletion experiments. Note that the differences in baseline values are linked to different times in vitro (1 day vrs 3 days) for overexpression and depletion experiments.

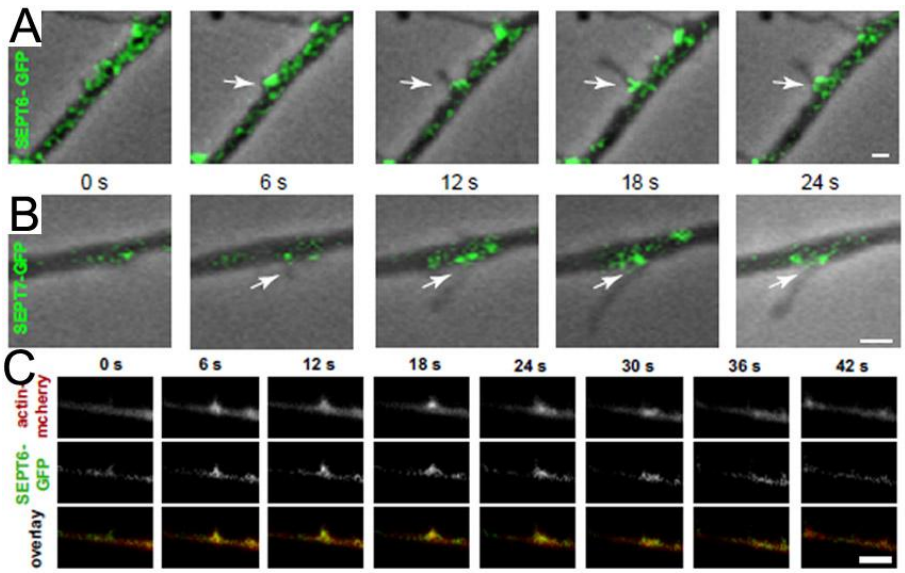

Figure 2. (A-B) phase contrast and GFP imaging of SEPT6 and SEPT7 during filopodia formation. (C) Imaging of GFP-SEPT6 and mCherry Actin. Note that SEPT6 is recruited to the forming actin patch (starting at 6 sec).

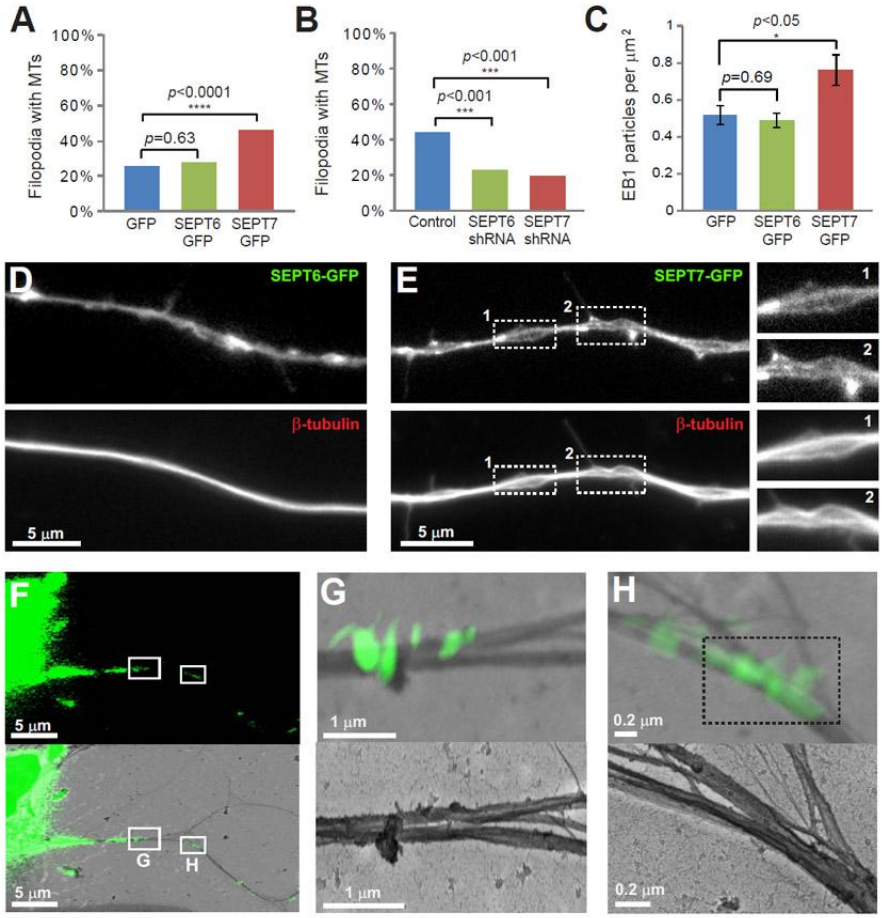

Figure 3. (A-B) quantification of the % of axonal filopodia containing microtubules in overexpression and depletion conditions as outlined in Figure 1. (C) Quantification of EB1 comets in axons in overexpression experiments. (D-E) The axonal microtubule array under conditions of SEPT6 and SEPT7 overexpression. Note the increase in debundling of the array in the SEPT7 overexpressing axon. (F-H) Correlative GFP-SEPT7 and microtubule ultrastructure in axons. Sites of GFP-SEPT7 accumulation correlate with microtubule debundling.

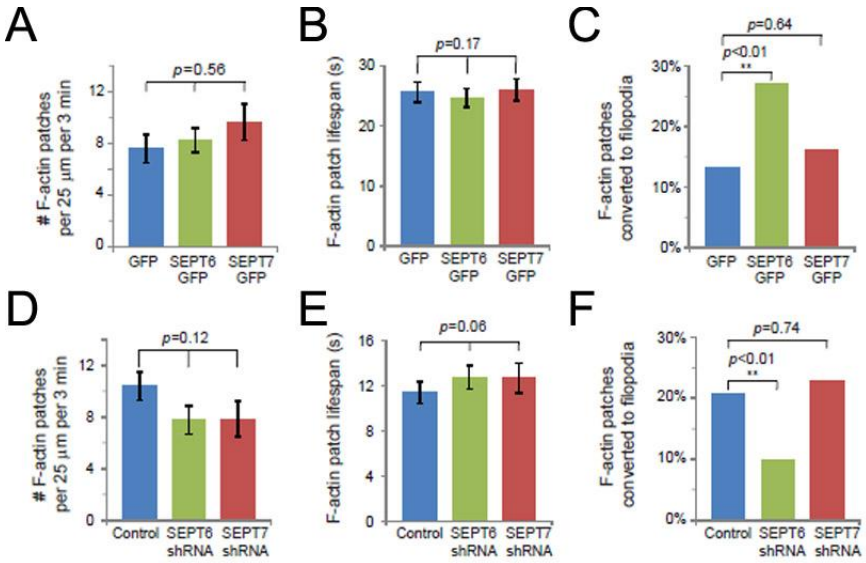

Figure 4. Quantification of the rate of formation of axonal actin patches (A,D), duration (B,E) and the emergence of filopodia from patches (C,F). (A-C) Overexpression of SEPT6 and SEPT7. (D-F) shRNA-mediated depletion of SEPT6 and SEPT7.

<u>Research Project 5: Project Title and Purpose</u>

Development of the Cardiac Ultrasound Pacemaker - There is an unmet need for a technology to reliably and painlessly pace the heart without any surgical implantation or intravascular catheter placement. Our objective is to develop a technology that would provide noninvasive, low infection risk, and reliable pacing for minutes to weeks in conscious patients requiring temporary or emergency pacing. We envision an ultrasound device that could be placed directly on the skin of the chest wall that would function as a pacemaker for the heart.

Anticipated Duration of Project

1/1/2010 - 12/31/2012

Project Overview

We will research and develop a completely non-invasive, fully ambulatory, and safe alternative pacing technology using externally applied ultrasound at FDA approved frequencies and intensities. The applied ultrasound device will be able to initiate periodic myocardial depolarization resulting in cardiac contraction thereby establishing a consistent and reliable pacing rhythm without need for the direct or indirect application of electric energy. In contrast to all other devices on the market, the technology proposed in this development effort is completely extracorporeal; an external, wearable ultrasound pacemaker.

A porcine model will be used for our experiments. The choice of a porcine model is supported by the literature since pigs and humans share similarities in terms of the anatomical heart size, location and position of the heart in the thoracic cavity, and intrinsic heart rate. Moreover, these

animals will be available for noninvasive testing at our institution. Porcine heart rhythm will be monitored using surface electrodes and a multi-channel electrocardiogram. An M-mode ultrasound imager will be used to identify a location on the chest wall that provides access to the myocardium with a minimum of obstructions. The external ultrasound probe will be placed on the chest surface with coupling gel. The ultrasound pulses will be synchronized with the native heart rhythm using an electrocardiogram to avoid inducing ventricular arrhythmia. Following FDA guidelines, only ultrasound intensity levels with a spatial peak temporal average of 720mW/cm2 or less will be used for the feasibility studies. For the feasibility studies ultrasound pulses will be delivered for one minute, at a pulse interval approximately 25% below the inherent cycle length, to initiate pacing at 20 beats per minute (bpm) faster than the average underlying heart rhythm of 70bpm. The ultrasound-initiated beats will be identified by the morphology of their QRS complexes and timing relative to the ultrasound pulse. A successful pacing protocol will be defined by a 70-100% capture of the delivered ultrasound pulses for three to five minutes. This will provide data on 270-450 successive stimulations for analysis. The heart rhythm will be monitored with the electrocardiogram for an additional 5 minutes to document whether any residual electrophysiologic effects from the ultrasound are present.

Principal Investigator

Andrew R. Kohut, MD, MPH
Assistant Professor of Medicine
Drexel University College of Medicine
Mail Stop 470
245 North 15th Street
Philadelphia, PA 19102-1192

Other Participating Researchers

Peter A. Lewin, PhD - employed by Drexel University
Peter B. Kurnik, MD, Steven P. Kutalek, MD - employed by Drexel University College of Medicine
Christopher Vecchio, PhD - employed by Spectrasonics Imaging, Inc.

Expected Research Outcomes and Benefits

Cardiac pacemakers have been in existence for almost 50 years. There are two categories of cardiac pacemakers, temporary and permanent. The most recent statistics indicate there are about 1.3 million temporary cardiac pacemakers used annually in the USA at a total cost of about $3.4 billion dollars. Globally, the figures are much higher. The two current techniques for temporary cardiac pacing involve the surgical use of intravascular catheters and leads or the use of transcutaneous electrical pacing, which is painful and impractical for prolonged utility. These approaches have not significantly changed in the last 40 years and are associated with a myriad of morbidity and mortality outcomes as well as high costs. Complications can include infection, drug toxicity, renal failure due to prolonged use of antibiotics, and death.

Our proposed ultrasound device will operate at intensities that follow current FDA guidelines. It will provide rapidly-deployable, noninvasive, painless pacing for minutes to weeks in conscious patients requiring temporary or emergency pacing. Temporary cardiac pacemakers often represent the first therapeutic approach for the ultimate correction of a serious cardiac problem or malady. Such situations often result from bradyarrhythmias myocardial infarction, drug toxicity, bloodstream infection, during patient transport in emergency situations, or in the aftermath of heart surgery. The medical complications and costs associated with current approaches represent a very poorly met medical need, ripe for improvement both in terms of clinical outcome and cost reduction. As a result of the development of the proposed technology, the need for painful and invasive temporary intravascular pacing catheters or transcutaneous electrical pacers would be reduced or eliminated.

Summary of Research Completed

Experimental System

We have assembled a prototype pacing ultrasound system for *in vivo* experimentation. Since our last progress report, this system has been upgraded to include a new power amplifier, dedicated oscilloscope, and an improved ECG monitor. The prototype system utilizes both 1.6 MHz 15mm diameter and 2.5 MHz 11mm diameter unfocused ultrasound probes. Future experiments will also include a recently-acquired 0.5MHz focused probe. The system includes gating and synchronization hardware to allow energy delivery during precise time intervals following each native porcine QRS complex (ventricular depolarization) in an effort to avoid inducing tachyarrhythmias via potential early afterdepolarizations (EADs) and delayed afterdepolarizations (DADs). The recent improvements have allowed us to use a wider range of excitation frequencies and probes and to better control the ultrasonic pulse amplitude. A diagram of the experimental system is shown in Fig. 1.

In vivo Experiments

Two modified animal protocols have also been introduced. These revised protocols were approved by the IACUC committee in July 2010 and September 2010. The protocols are described in more detail below.

I. A series of experiments was performed on 4 porcine models utilizing a protocol approved by our University's Institutional Animal Care and Use Committee (IACUC). The following protocol was used for these animals:

1. Placed 3 ECG electrodes on the shaved chest wall of anesthetized animal
2. Connected ECG electrodes to ECG monitor and ECG monitor to QRS detection, gating, and stimulating ultrasound hardware
3. Placed ultrasound transmission gel and ultrasound probe on chest wall
4. Synchronized ultrasound pulse delivery to native heart rhythm to avoid inducing ventricular arrhythmia. The native porcine heart rate was slightly higher than anticipated in some instances, approximately 120-140 bpm.
5. A fixed frequency ultrasound probe of either 1.6 MHz or 2.5 MHz was applied using Aquasonic 100® ultrasound transmission gel at 4 different locations on the chestwall: (1)

midclavicular line at the level of the 6-8th intercoastal space, (2) midaxillary line at the level of the 6-8th intercoastal space and (3) midclavicular line from subcoastal angulation towards the ipsilateral shoulder. These sites of stimulation were selected using 2D echocardiography.

a. Ultrasound pulses were delivered for one minute bursts, with pulse delays of 0, 0.05, 0.10, 0.15, 0.2 and 0.3 seconds, following the peak amplitude of the QRS complex. The pulse durations were set at 2, 4, 8, 10 and 14 milliseconds, while targeting a sound pressure level of 2.5-3.5MPa (megapascal) at the sites of stimulation.
b. Two animals were exposed to ultrasound pulses delivered:
    i. 1.6 MHz with pulse delay of 0.2 sec and pulse duration of 2 msec
    ii. 1.6 MHz with pulse delay of 0.2 sec and pulse duration of 3 msec
    iii. 1.6 MHz with pulse delay of 0.2 sec and pulse duration of 4 msec
    iv. 1.6 MHz with pulse delay of 0.2 sec and pulse duration of 10 msec
    v. 1.6 MHz with pulse delay of 0.2 sec and pulse duration of 12 msec
    vi. 1.6 MHz with pulse delay of 0.2 sec and pulse duration of 14 msec
    vii. 1.6 MHz with pulse delay of 0.3 sec and pulse duration of 2 msec
    viii. 1.6 MHz with pulse delay of 0.3 sec and pulse duration of 4 msec
    ix. 1.6 MHz with pulse delay of 0.3 sec and pulse duration of 10 msec
    x. 1.6 MHz with pulse delay of 0.3 sec and pulse duration of 12 msec
    xi. 1.6 MHz with pulse delay of 0.3 sec and pulse duration of 14 msec
c. Two animals were exposed to ultrasound pulses delivered:
    i. 2.5 MHz with pulse delay of 0 sec and pulse duration of 2 msec
    ii. 2.5 MHz with pulse delay of 0 sec and pulse duration of 4 msec
    iii. 2.5 MHz with pulse delay of 0 sec and pulse duration of 8 msec
    iv. 2.5 MHz with pulse delay of 0 sec and pulse duration of 10 msec
    v. 2.5 MHz with pulse delay of 0 sec and pulse duration of 14 msec
    vi. 2.5 MHz with pulse delay of 0.20 sec and pulse duration of 2 msec
    vii. 2.5 MHz with pulse delay of 0.20 sec and pulse duration of 4 msec
    viii. 2.5 MHz with pulse delay of 0.20 sec and pulse duration of 8 msec
    ix. 2.5 MHz with pulse delay of 0.20 sec and pulse duration of 10 msec
    x. 2.5 MHz with pulse delay of 0.20 sec and pulse duration of 14 msec
    xi. 2.5 MHz with pulse delay of 0.30 sec and pulse duration of 2 msec
    xii. 2.5 MHz with pulse delay of 0.30 sec and pulse duration of 4 msec
    xiii. 2.5 MHz with pulse delay of 0.30 sec and pulse duration of 8 msec
    xiv. 2.5 MHz with pulse delay of 0.30 sec and pulse duration of 10 msec
    xv. 2.5 MHz with pulse delay of 0.30 sec and pulse duration of 14 msec

6. The native heart rhythm was recorded using 3-lead surface ECG rhythm strip.
7. The ECG rhythm strips were reviewed and analyzed for the presents of ultrasound-initiated beats after each ultrasound pulse parameter change.
8. The heart rhythm was monitored with the electrocardiogram for an additional 5 minutes to document whether any residual electrophysiologic effects from the ultrasound are present.

II. A second series of experiments was performed on 2 porcine models utilizing a protocol approved by our University's Institutional Animal Care and Use Committee (IACUC). The following protocol was used for these animals:

1. Each animal was anesthetized, intubated and placed on a mechanical respirator
2. Placed 3 ECG electrodes on the shaved chest wall of anesthetized animal.
3. Connected ECG electrodes to ECG monitor and ECG monitor to QRS detection, gating, and stimulating ultrasound hardware
4. Sternotomy performed using standard sterile surgical technique. The pericardial sack was resected and a 3-4 cm diameter of the epicardial surface of the left ventricle was exposed.
5. A fluid-filled latex sack, as a functional spacer, was placed in direct contact with the surface of the left ventricle. A fixed frequency ultrasound probe of either 1.6 MHz or 2.5 MHz was applied to the latex sack.
6. Synchronized ultrasound pulse delivery to native heart rhythm to avoid inducing ventricular arrhythmia. The native porcine heart rate was slightly higher than anticipated in some instances, approximately 120-140 bpm.
    a. Ultrasound pulses were delivered for one minute bursts, with pulse delays of 0.2 and 0.3 seconds, following the peak amplitude of the QRS complex. The pulse durations were set at 2, 4, 10, 12 and 14 milliseconds, while targeting a sound pressure level of 2.5-3.5MPa (megapascal) at the sites of stimulation.
    b. Each animal was exposed to ultrasound pulses delivered:
        i. 1.6 MHz with pulse delay of 0.2 sec and pulse duration of 2 msec
        ii. 1.6 MHz with pulse delay of 0.2 sec and pulse duration of 4 msec
        iii. 1.6 MHz with pulse delay of 0.2 sec and pulse duration of 10 msec
        iv. 1.6 MHz with pulse delay of 0.2 sec and pulse duration of 12 msec
        v. 1.6 MHz with pulse delay of 0.2 sec and pulse duration of 14 msec
        vi. 1.6 MHz with pulse delay of 0.3 sec and pulse duration of 2 msec
        vii. 1.6 MHz with pulse delay of 0.3 sec and pulse duration of 4 msec
        viii. 1.6 MHz with pulse delay of 0.3 sec and pulse duration of 10 msec
        ix. 1.6 MHz with pulse delay of 0.3 sec and pulse duration of 12 msec
        x. 1.6 MHz with pulse delay of 0.3 sec and pulse duration of 14 msec

<u>Results</u>

Unfortunately, the results of our experiments to date have been inconclusive. No clearly identifiable ultrasound-initiated beats were seen in the ECG recordings. In an effort to improve our system, we have mathematically modeled the generated ultrasound beam intensities and accounted for the energy losses incurred as the beam passes through the porcine chest wall and cardiac tissue layers. Our data from this model suggests that lower frequency ultrasound may be more likely to deliver the required radiation force to the epicardial and endocardial layers of the heart.

We have specified and purchased a new lower frequency (0.5MHz), focused ultrasound probe. This is a high-efficiency, broad bandwidth transducer designed for high-intensity focused ultrasound experiments. This new probe will allow us to investigate the utility of lower

frequency ultrasound excitations and, as a result of focusing, allow us to overcome the effects of attenuation to apply higher ultrasound intensities at the epicardial surface.

We are currently revising and modifying the details of our experimental approach in light of the recent results and modeling predictions.

Figure 1

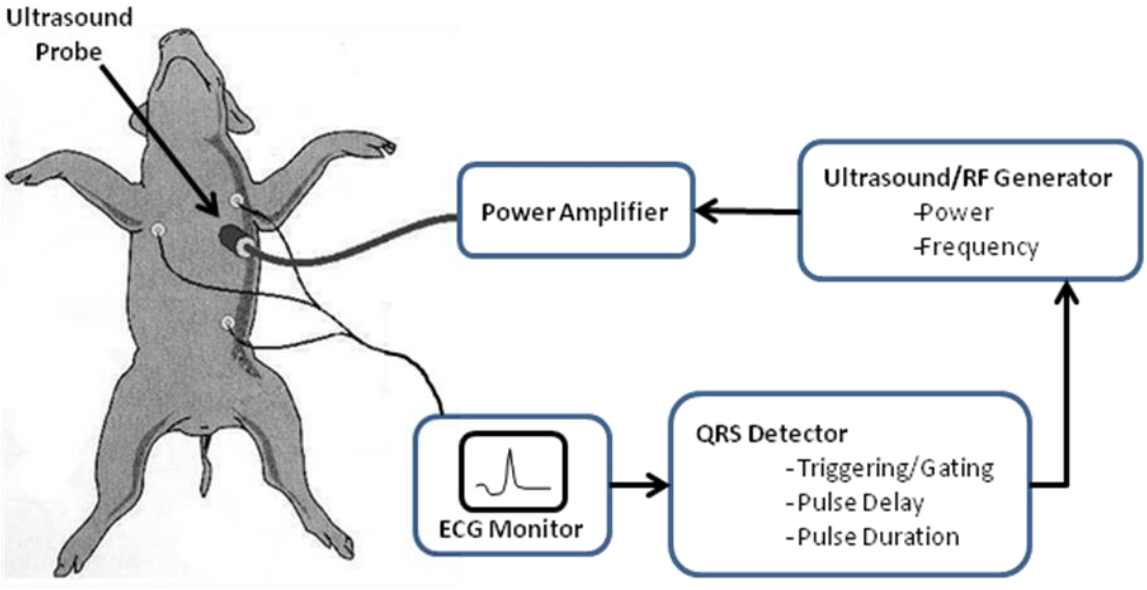

Fig. 1. Diagram of experimental ultrasonic pacing system.

Research Project 6: Project Title and Purpose

Human Lung Progenitor Cells for Pulmonary Tissue Engineering and Regenerative Medicine - The purpose of this interdisciplinary research is to isolate and study human lung-specific somatic progenitor cells. These cells can be used to engineer high-fidelity distal pulmonary constructs (alveolar forming units, AFUs) for studying basic mechanisms of lung development and ultimately, for treating currently incurable lung diseases, such as in newborns (e.g., pulmonary hypoplasias) and/or in adults, (e.g., chronic obstructive pulmonary disease (COPD), such as emphysema). Moreover these AFUs can also lead to a commercializable tissue-engineered product for use as models in accelerated drug discovery (e.g., improved anti-asthmatics), in understanding common lung infections (e.g., pneumonia/tuberculosis), or in toxicity studies (e.g., asbestos/vapor inhalation).

Anticipated Duration of Project

1/1/2010 - 12/31/2011

Project Overview

Project goals will be achieved through three specific aims:

Aim1: *To isolate and characterize human lung progenitor cells (hLPCs) derived from distal airways/alveoli.* Using techniques established in non-human mammalian lung, we will isolate, culture and characterize hLPCs from freeze-thawed fragments of human distal lungs, obtained from anonymous donors from the Tissue Bank.

Aim 2: *To develop an optimized regimen for the directed differentiation of hLPCs into diverse distal pulmonary alveolar cells.* The main goal of Aim 2 is to develop an optimized regimen for the directed differentiation of hLPCs into diverse distal pulmonary alveolar cells, specifically AE2 cells and endothelial cells (ECs) and other mesenchymal cells.

Aim 3*: To assess assembly of hLPC into "alveolar forming units" upon seeding into tissue-engineered permissive matrices*. In this aim, we will explore the functional assembly of hLPC derivatives into vascularized, surfactant synthesizing "alveolar forming units," similar to our prior work with fetal murine lung cells as a model system.

In this project we will synergistically leverage the unique expertise of two laboratories in an effort to propel Drexel to the apex of personalized lung tissue engineering and regenerative medicine. Moreover the availability of tissue samples (biopsies) from individual patients opens the realm of "personalized" regenerative medicine, the possibility to study patient-centered lung development in health and disease and/or producing autologous lung cells for transplantation back into the patient.

Principal Investigator

Peter I. Lelkes, PhD
Calhoun Chair Professor of Cellular Tissue Engineering
Drexel University
3141 Chestnut Street, Bossone Room 707
Philadelphia, PA, 19104

Other Participating Researchers

Edward S. Schulman, MD, PhD - employed by Drexel University College of Medicine

Expected Research Outcomes and Benefits

We fully expect to be able to isolate spore-like pulmonary stem cells, to be able to differentiate these stem cells toward pulmonary lineages, and to reconstruct distal airways (alveoli like structures), structurally and functionally.

Summary of Research Completed

In the first 9 months of the grant we attempted to recapitulate previous attempts at isolating a stem cell from the adult rat and human lung following a series of unpublished and published single step protocols developed mainly for rats and mice. In our hands, these single-step digestion protocols were too harsh yielding few viable, mostly fibroblastic cells. Cell numbers

and viability were significantly improved by decreasing digestion times from 45 min to 15 min and increasing the number of sequential short-time digestions (from one to four times). Below are examples of the type of heterogeneous population that was obtained from our modified digestion protocol (Figure 1).

At the time we were performing these isolations in rats, most work by others was being performed on mice with little consensus as to the phenotypic markers for the lung stem cells.

Following successful isolation and culture of a heterogeneous population of adult rat lung cells, we tested the procedure on adult human lung. With the application of the above digestion protocol we were able to isolate mainly fibroblast-like cells (Figure 2). We then further optimized the concentration of enzyme, and the length of digestion to obtain a heterogeneous population of adult human lung cells. Up to this point the only cells reported to be isolated from human lung came from the conducting airways, and not the gas exchanging epithelium. Therefore a further isolation with Fluorescently Activated Cell Sorting (FACS), or Magnetically Activated Cell Sorting (MACS) was not needed.

A recent paper by Kajstura et al. (2011) has shown their lung "stem cells" were CD117+ (aka: c-Kit+). CD117 is also a marker in particular for Mast Cells (according to Dr. Schulman's work), and Bone Marrow Progenitors (usually used as a positive control in staining). We are now using our constant supply of healthy human lung tissue to isolate the human lung "stem cells" according to the procedures described by Kajstura et al. Our aim is to unequivocally show that these cells can be cultured in F12 medium supplemented with 10% Fetal Calf Serum. We expect that at isolation the majority of the CD117+ cells will be mast cells. As Kajtura et al. reported no presence of mast cells in their culture, we surmise that this was not due to any sorting technique used, but due to the fact that mast cells will die in a culture that does not include very specific growth factors and cytokines. Therefore we aim to put the entire population of CD117+ cells in culture as a selection step for the "stem cells."

For the initial validation, we used Flow Cytometry to analyze CD117 expression across different elutriation fractions. These fractions were then split into three groups: unstained, isotype control, and stained cells. The antibody was anti-human CD117, and the appropriate isotype control was obtained from Milteny Biotech (anti Mouse IgG1). The results from the flow cytometry analysis indicate significant numbers of CD117+ cells in fractions C and D (Figure 3).

Having successfully demonstrated the presence of CD117+ cells in our primary isolates the next step will be to sterilely sort CD117+ cells, and put them in culture. Future experiments will include a marker for mast cells such as Tryptase, or a marker for stem cells such as Oct4. By double/triple staining, we will be able to distinguish between lung stem cells, and mast cells (which would still be alive immediately following the isolation but absent upon prolonged culture). Once in culture the cell's proliferation potential and pluripotency marker/gene expression will be characterized.

<u>Impact of the CURE-Award:</u> The work funded through this award was the basis for a recently awarded, 3 year National Aeronautics and Space Administration-Graduate Student Research Assistant (NASA-GSRA) fellowship that will fund Collin Stabler's PhD studies. Furthermore

this work will serve as the basis for a grant application to the National Institute of Health (to be submitted October 1, 2011). In addition, part of the work will be presented at the Vermont Lung Stem Cell and Engineering Conference, July 25-28.

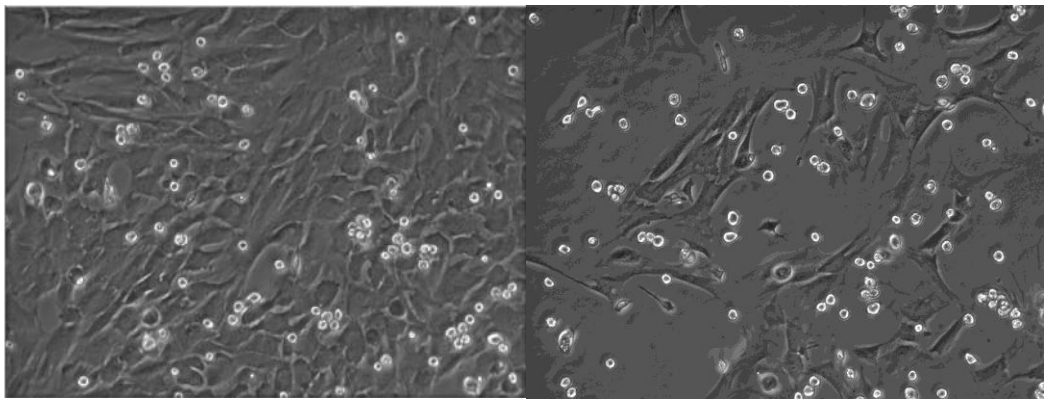

Figure 1: Rat lung cells. Both figures are at a 10X magnification.

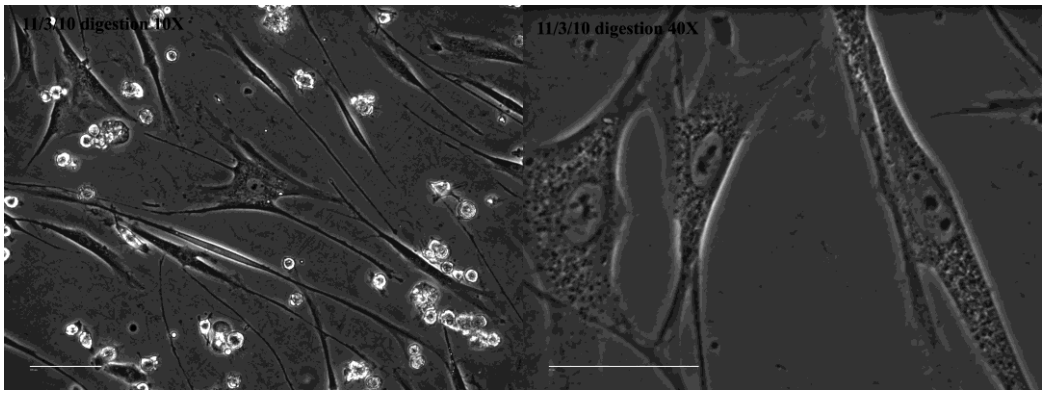

Figure 2: Human lung cells. The figure on the left is at a 10X magnification with the scale bar at 100um. The figure on the right is at a 40X magnification with the scale bar at 100um.

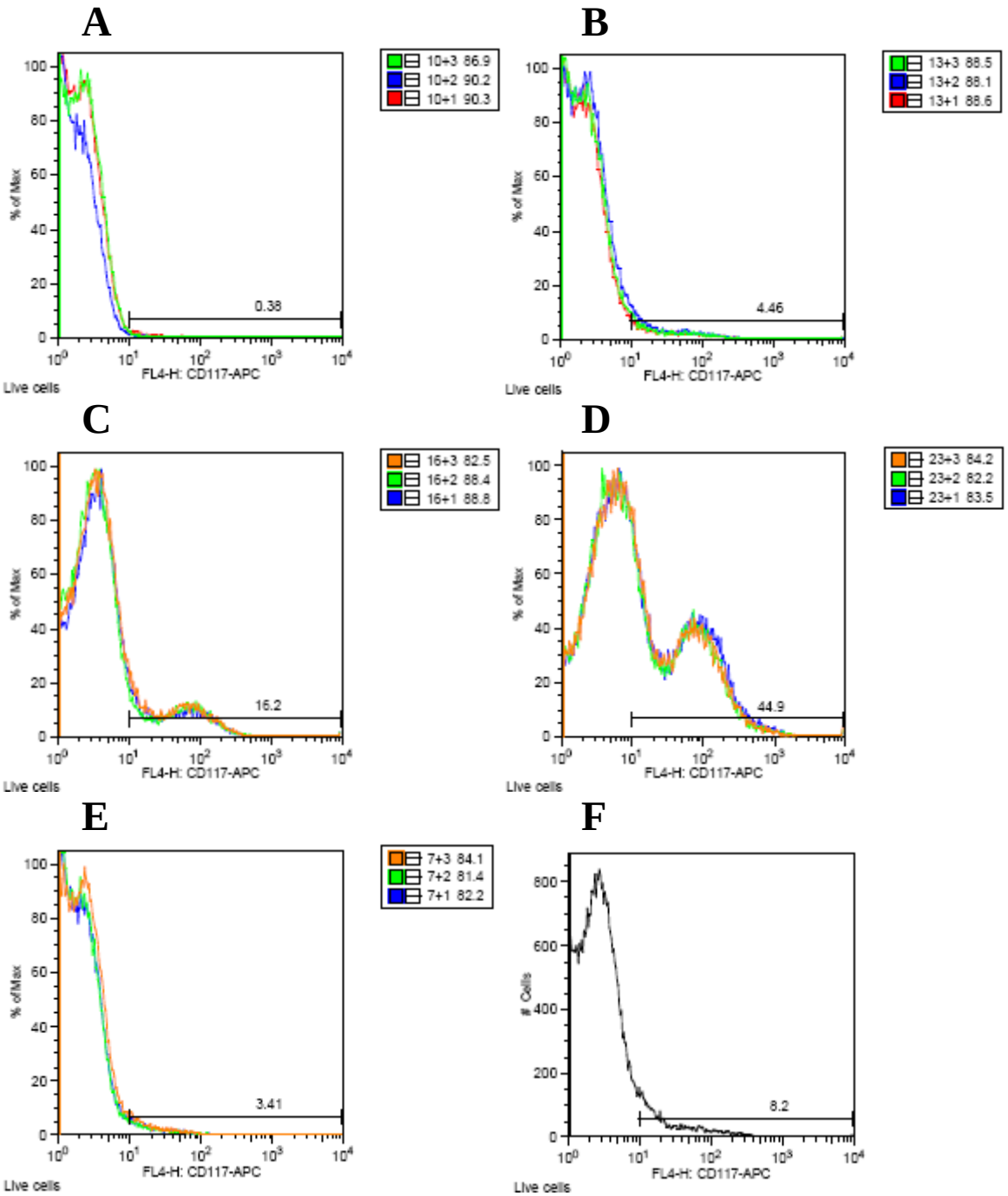

Figure 3: Graphs are of the raw data acquired from the positively stained fractions. A: Fraction "10-12", B: Fraction "13-15", C: Fraction "16-18", D: Fraction "23-25", E: Fraction "7-9", F: Fraction "19-22".

Research Project 7: Project Title and Purpose

Novel Oligomers Targeting AMPA Receptors as Therapeutics for ALS - In this project we will evaluate the efficacy of compounds we have developed called splice modulating oligomers (SMOs), which dramatically decrease flip/flop levels of targeted GluR AMPA subunits, to improve motor function and prolong lifespan in transgenic ALS mice. SMOs are compounds that function by binding to their target pre-mRNA, and redirecting pre-mRNA splicing by the spiceosomal complex in a predictable fashion. Due to recent improvements in chemistry, SMOs show extraordinary specificity, potency, and resistance to degradation. We propose that our SMOs could ultimately be used clinically as neuroprotective agents for treating amyotrophic lateral sclerosis (ALS), by reducing calcium influx in motor neurons (MNs) and breaking the feedback cycle involved in glutamate-mediated excitotoxicity.

Duration of Project

1/1/2010 - 6/30/2011

Project Overview

Amyotrophic lateral sclerosis (ALS) is characterized by the progressive and selective loss of motor neurons (MNs) in the motor cortex, brainstem, and spinal cord, resulting in patient death typically 3-5 years after diagnosis. Glutamate-mediated excitotoxicity in the CNS has been firmly implicated as a major contributor to the manifestation of both sporadic and familial ALS. Excitotoxicity is the result of excessive Ca2+ influx into MNs, coupled with the diminished capacity of MNs to handle Ca2+ overload, which appears to result in excessive Ca2+ entering mitochondria and the release of harmful molecules from mitochondria, which appear to damage glutamate transporters on adjacent astrocytes. This sets up a disastrous feedback cycle in which synaptic glutamate levels continually rise, further increasing Ca2+ influx and exacerbating mitochondrial Ca2+ overload, ultimately leading to MN cell death. Therefore, drugs which effectively lower Ca2+ influx in the MNs during excitatory activity offer great promise as therapeutics for ALS.

In this project we will evaluate the efficacy of our lead SMO after continuous ICV delivery to reduce GluR3-flip isoform expression in relatively short-term 3 wk trials in ALS mice; focusing on the dose-response of GluR3-flip knockdown throughout the CNS. We will then conduct longer-term ICV delivery trials of the efficacy of our lead SMO in ALS mice; focusing on delaying motor deficits and increasing lifespan.

Principal Investigator

Gordon J. Lutz, PhD
Associate Professor
Drexel University College of Medicine
245 N. 15th St.
New College Building, MS 497
Philadelphia, PA. 19102

Other Participating Researchers

Melanie K. Tallent, PhD, Terry Heiman-Patterson, MD, PhD - employed by Drexel University

Expected Research Outcomes and Benefits

We will evaluate the efficacy of our lead SMO after continuous ICV delivery to reduce GluR3-flip isoform expression in relatively short-term 3 week trials in ALS mice; focusing on the dose-response of GluR3-flip knockdown throughout the CNS.

We will also conduct longer-term ICV delivery trials of the efficacy of our lead SMO in ALS mice, focusing on delaying motor deficits and increasing lifespan.

The proposed experiments are all empirical in nature and are product-driven with the express intent to provide 'proof of principle' that our novel drug candidates are efficacious in improving motor function and lifespan in an animal model of ALS. There are no drugs in clinical usage that specifically decrease AMPA channel GluR-flip subunit expression or increase desensitization kinetics. The SMOs in this project may ultimately be used clinically as neuroprotective agents for treating ALS, by reducing Ca^{2+} influx in MNs and breaking the feedback cycle involved in glutamate-mediated excitotoxicity.

Summary of Research Completed

METHODS

<u>Animals</u>
Two strains of adult ALS mice were used. For the continuous ICV delivery experiments we used congenic G93A SOD1 ALS mice backcrossed to a C57Bl/J6 background strain for over 20 generations (B6.Cg-Tg(SOD1*G93A)1Gur/J; Jackson Labs stock 004435). These ALS/B6 mice carry 25 copies of human mutant (G93A) SOD1, which is the genetic basis for their MN degenerative phenotype. ALS mice of this strain, referred to simply as SOD1/B6 ALS mice, were derived from in-house breedings between males hemizygous for the human mutant G93A SOD1 transgene and wild-type C57Bl6 females. Genotype was established post-weaning using a standard Real-time PCR protocol to detect the mutant SOD1 gene. For the bolus lumbar spinal infusion studies we switched to the G93A SOD1 ALS mice bred on a mixed SJL/B6 background (Jax; B6SJL-Tg(SOD1*G93A)1Gur/J). These ALS mice typically survive to about 128.9 (+/-9.1 d). ALS mice of this strain, referred to simply as ALS/B6-SJL mice, were purchased in sets of littermates from Jackson Labs at about 5-6 weeks of age.

<u>ALS mouse experimental groups</u>
Continuous ICV delivery using Alzet cannulae/minipumps. SOD1 ALS-B6 littermates were randomly assigned into two groups: (i) GR1 SMO, and (ii) saline.
Bolus spinal injections. SOD1 ALS-B6/SJL littermates were randomly assigned into two groups: (i) GR1 SMO, and (ii) saline.

GR1: This SMO targeted the 3' splice site and adjacent exonic splice enhancer motifs of the GluA1-flip pre-mRNA where its sequence is divergent from all other GluA isoforms.

Alzet cannulae/osmotic pump continuous ICV delivery of SMOs

Mice were implanted with a cannula in the lateral ventricle connected to an Alzet minipump for continuous delivery of SMOs to the CSF. Mice were anaesthetized with isoflurane and a cannula (Alzet, Brain Infusion Kit 3) was inserted stereotaxically into the right lateral ventricle with the cannula tubing connected to a sub-cu implanted Alzet minipump (1004), pre-loaded with SMO or saline. The entire system was internalized beneath the skin. Prior to implant, pumps were filled with SMO or saline and equilibrated in sterile saline at 37oC for 24 h. The Alzet pump delivered 2.4+ 0.2 μL per day with enough volume (100 μL) for at least 28 d of continuous infusion. In the ALS mouse trials, the first pump and cannulae were implanted at 62 d of age. The pump was replaced after 4 weeks (day 90) and 8 weeks (day 108) with a rapid minor surgery where the expiring pump was simply replaced with a new pump that was reconnected to the original cannula tubing. Then after an additional 4 wks (day 146), another minor surgery was performed where the pump was removed, and the cannulae tubing was cutoff close to the cannulae insertion point, and the cannulae port was sealed shut. Incisions were closed and mice quickly recovered after removal from anesthetic.

Bolus lumbar spinal infusions of SMOs

Mice were anaesthetized with isoflurane and a small 1 cm incision was made to expose the musculature above the L5-L6 region of the spinal cord. A 32 gauge needle mounted on a 25 μL Hamilton syringe was inserted slowly at a 45° angle into the L5-L6 gap until the needle tip punctured the dura (detected by a tail flick reflex) and then the angle was lowered and the needle was advanced another ~2-3 mm into the spinal column. A 6 μL solution of SMO or saline was delivered into the CSF of the spinal column slowly over a 3 min period and then the needle was held in place for 30 sec prior to removal. The small incision was closed with a single stitch and mice recovered to full ambulation within 5 min.

RESULTS

Efficacy of GR1 SMO throughout the CNS of normal adult mice after continuous ICV delivery

Because SMOs do not cross the blood brain barrier, they must be delivered directly to the CSF. Implantation of cannulae in the spinal cords of mice for continuous long-term delivery of drugs is technically difficult and damaging to the spinal cord. Thus, we elected to begin our studies of SMO efficacy using continuous ICV delivery. Using a stereotaxic system, normal C57Bl6 adult (90 d old) mice were implanted with cannulae in their right lateral ventricle, which was connected through tubing to a sub-cu embedded osmotic minipump (see Methods), which was pre-loaded with either the GR1 SMO or saline. The dose-response profile of GR1 after 4 weeks of continuous ICV delivery system was determined by measuring GluA1-flip and GluA1-flop transcript levels throughout the CNS. Dosing rates of GR1 from 1-20 μg per day for 4 weeks all produced significant decreases in GluA1-flip in all regions of brain and spinal cord compared to saline-treated controls (Fig. 1a). Given that our ICV dosing in ALS mice will be continuous for 12 weeks, we used these 4 week dosing data in normal mice to select 10 ug/d for the our efficacy studies of GR1 in ALS mice.

Influence of continuous ICV delivery of GR1 SMO on motor function and lifespan of ALS mice
The B6 congenic ALS mice were dosed with the GR1 SMO (10 μg per day) for 12 weeks, beginning at 62 days of age. Although the number of mice is clearly far too low for definitive conclusions (N = 4 mice per group), the GR1 SMO-treated mice still showed a significant increase in lifespan compared to saline-treated controls (Fig. 1b). The GR1 SMO-treated mice also showed a delay in disease onset, assessed by a delay in abnormal splay response (Fig. 1c; higher splay score indicates hindlimb motor weakening), and improved motor function for other tests including beam walk and ladder climbing ability (not shown).

Influence of bolus spinal delivery of GR1 SMO on motor function and lifespan of ALS mice
The fact that ALS pathology, including loss of MNs, progresses in a dorsal to proximal direction in MNs of ALS mice, provided strong validation that periodic bolus spinal injections of GR1 may produce a more potent reduction in ALS disease progression than continuous ICV delivery, and has many potential advantages for clinical application.

ALS-B6/SJL mice were given a spinal lumbar bolus injection of 50 μg of GR1 at age 60 days (pre-symptomatic) and a follow up injection of 25 μg of GR1 at age 90 days (post symptomatic). Littermate control mice were given saline injections at the same time point. A full battery of phenotypic and motor tests was performed 2 times per week on all mice from age 50 days until endstage. ALS-B6/SJL mice that received spinal bolus injections of GR1 lived to 129.3 ± 2.6 d, which was 7.6 days longer than their saline-treated littermates (Fig. 2).

Bolus spinal injections of GR1 also significantly delayed the onset of both forelimb and hindlimb tremor in ALS mice (Fig. 3). Spinal bolus injections of GR1 also significantly delayed the progression of deficits in the splay reflex response when analyzed over the full time course from 50 days of age to endstage compared to their saline-injected littermates (Fig. 4a). In addition, analysis at specific stages showed that GR1 significantly delayed progression to a mean splay score of 1 as well a splay score of 2 (Fig. 4b).

Spinal administration of GR1 significantly delayed deficits in beam walk performance when analyzed over the full time course from 50 days of age to endstage, compared to their saline-injected littermates (Fig. 5a). In addition, GR1 significantly delayed progression to mean beam scores of 1 and 2 (Fig. 5b). Similar to its effect on both splay and beam indicators of disease progression, administration of GR1 also significantly delayed deficits in upward and downward ladder climbing ability (Fig. 6).

It has long been known that ionotropic AMPA GluA subunits are alternatively spliced at their flip/flop exon, and that AMPA channels comprised of different GluA flip and flop splice variants have substantially different kinetics. Given that AMPA channels clearly play a pivotal role in the process of excitotoxicity, which has been implicated in a wide range of neurological diseases, it is remarkable that there are no drugs in clinical usage that regulate GluA alternative splicing. Here we showed that a novel SMO, GR1, which potently and specifically reduced the expression of GluA1-flip, significantly improved motor function and increased the lifespan of ALS mice after just two bolus injections into the lumbar spinal cord. These data confirm previous work implicating AMPA-Rs as having a pivotal role in producing excessive Ca2+ influx in MNs, and triggering excitotoxicity. Our innovative approach to AMPA channel modulation provided the

first opportunity to evaluate the impact of direct manipulation of GluA flip/flop alternative splicing on ALS disease progression. Our data, showing significant efficacy of SMOs after periodic intrathecal bolus injections, are the first of their kind in rodents, and pave the way toward clinical usage of SMOs for treating both FALS and SALS patients.

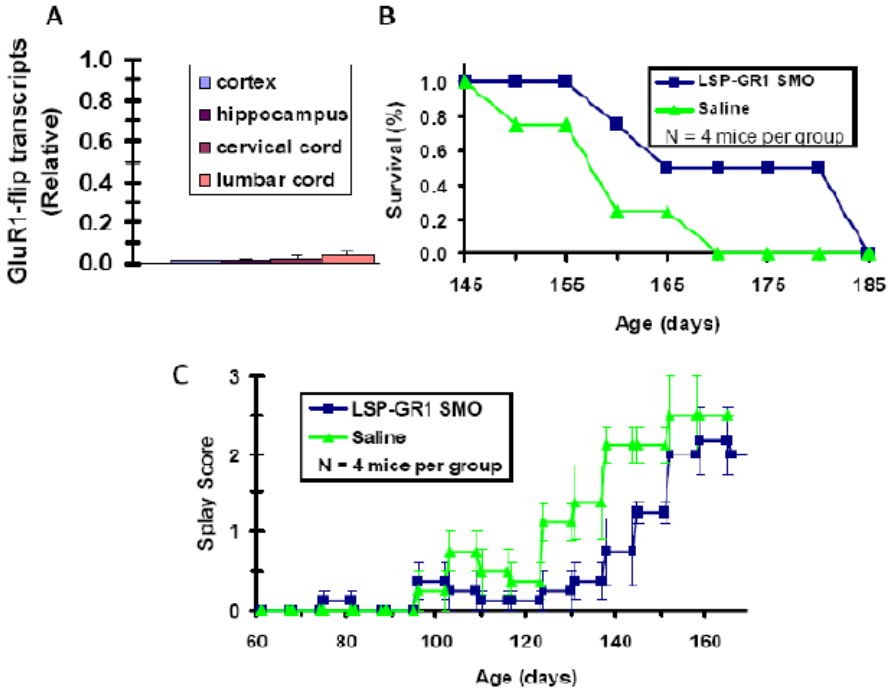

Figure 1. **(A)** GluR1-flip transcripts are nearly completely depleted in the CNS after 4 wk continuous ICV infusion of GR1 in normal mice (10 µg/d; N=3 mice). **(B-C)** Continuous 12 wk ICV infusion of GR1 beginning at 62 days of age in ALS mice significantly increased lifespan **(B)**, and delayed disease onset, based on the delay in abnormal splay response **(C)**.

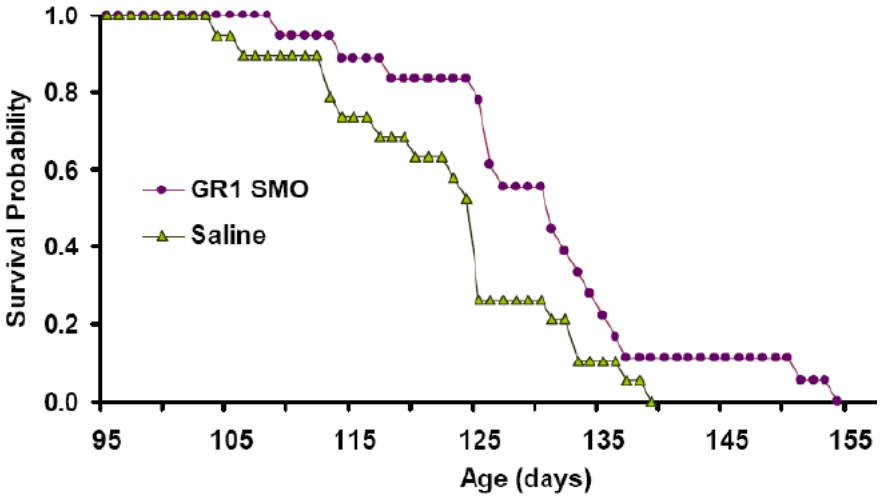

Figure 2. Kaplan-Meier survival plot of ALS mice treated with spinal bolus injections of GR1 increased longevity compared to their saline-injected littermates. At 60 days of age, mice were injected with 50 µg of SMO, followed at 90 days with a 25 µg injection. GR1 delayed death in

ALS mice ($p < 0.05$, n = 19 for saline and n = 18 for GR1-treated). Same cohort of mice are shown for all of the following figures.

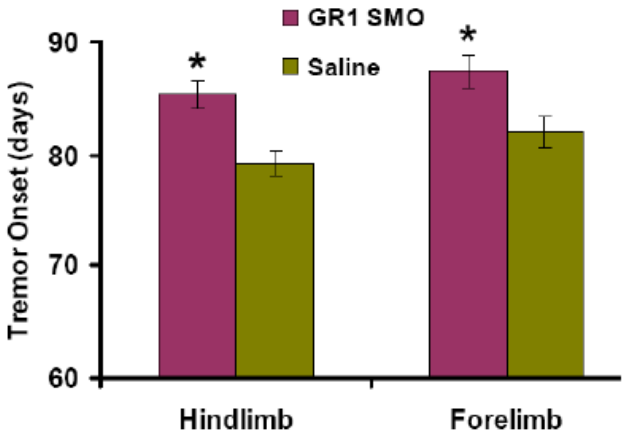

Figure 3. Both hindlimb and forelimb tremor onset was delayed after bolus spinal injections of GR1 in ALS mice compared to their saline-treated littermates. In GR1-treated ALS mice, mean age at which a tremor was first observed was significantly delayed in both hindlimb ($p < 0.001$) and forelimb ($p < 0.01$). GR1-treated mice (n = 18) and saline-injected littermates (n = 19).

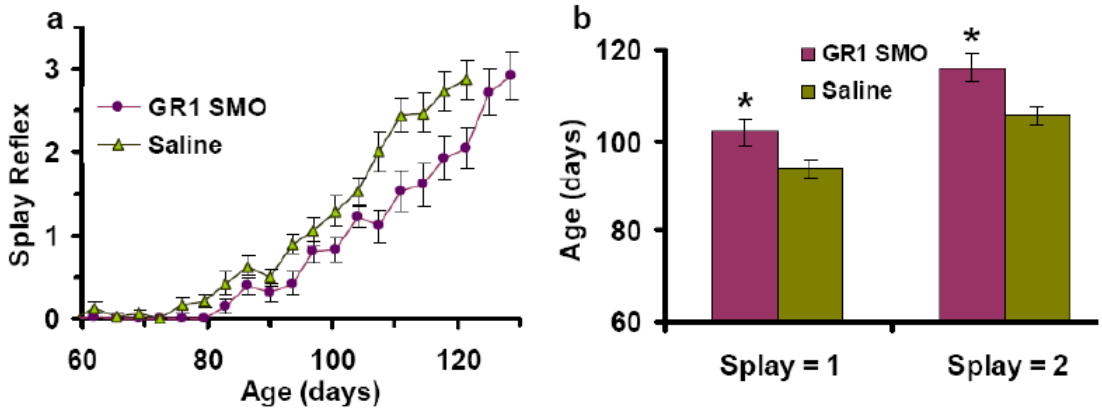

Figure 4. Deficits in splay reflex were delayed after bolus spinal injections of GR1 in ALS mice compared to their saline-treated littermates. **a.** Splay reflex was assessed across the lifespan of ALS mice from P60 to the time-point when 50% of each group had died. GR1-treated mice showed a significant delay in onset of splay deficit ($p < 0.005$). **b.** A significant delay in onset of splay scores of 1 ($p < 0.05$) and 2 ($p < 0.01$) was observed in GR1-treated mice. GR1-treated mice (n = 18) and saline-injected littermates (n = 19).

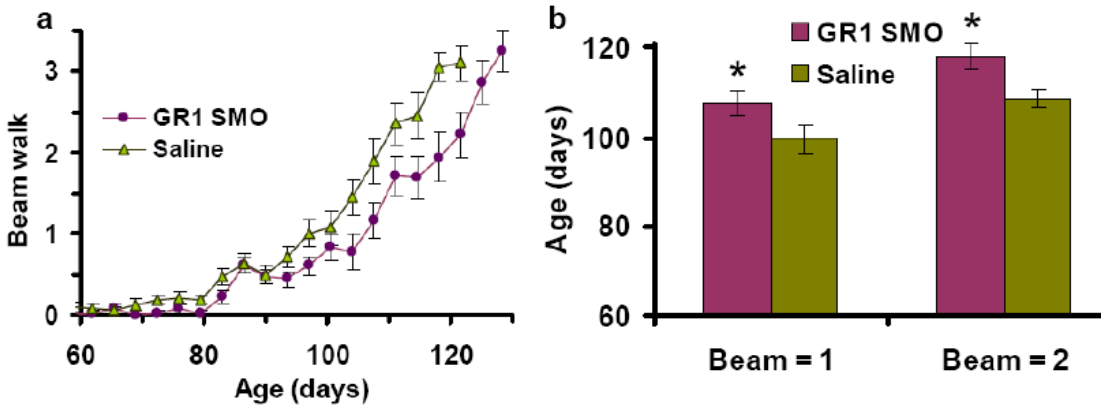

Figure 5. Deficits in beam walk performance were delayed after bolus spinal injections of GR1 ALS mice compared to their saline-treated littermates. **a.** Deficits in beam walking from P60 to time of death of 50% of each cohort showed a delay in progression in GR1-treated mice ($p < 0.01$). **b**. Mean time of onset of a beam score of 1 ($p = 0.049$) and 2 ($p = 0.009$) were significantly delayed in ALS mice treated with GR1 versus their saline-treated littermates. GR1-treated mice ($n = 18$) and saline-injected littermates ($n = 19$).

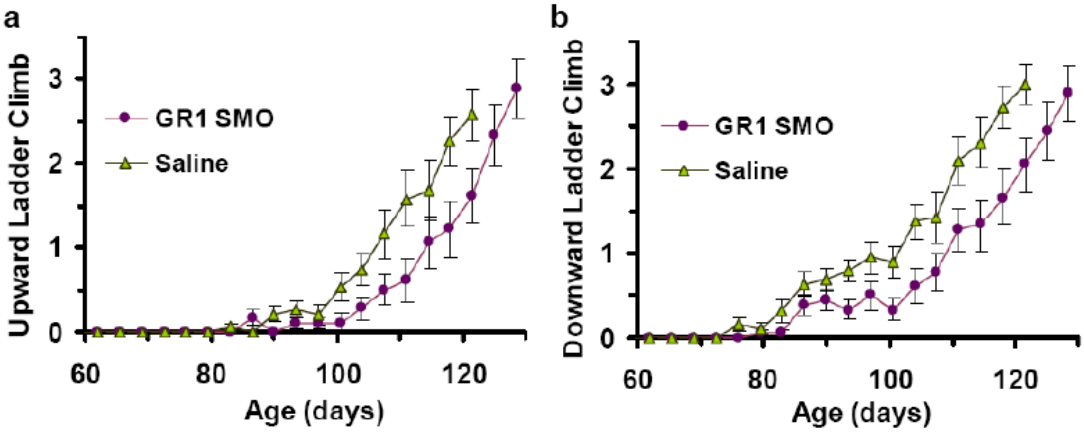

Figure 6. Deficits in both upward and downward ladder climbing capacity were delayed after bolus spinal injections of GR1 in ALS mice compared to their saline-treated littermates. **a.** Progression of deficits in upward ladder climbing was significantly delayed in mice administered GR1 ($p < 0.05$). **b.** ALS mice treated with GR1 also show improvement in downward ladder climbing compared to saline-treated mice ($p < 0.01$). GR1-treated mice ($n = 18$) and saline-injected littermates ($n = 19$).

Research Project 8: Project Title and Purpose

Neuronal Substrates of Cognitive Flexibility - Cognitive flexibility is the capacity to alter behavior to meet unexpected challenges, and is an essential aspect of adaptive behavior. Unfortunately, deficits in this capacity are hallmarks of various psychological and neurodevelopmental disorders including schizophrenia, obsessive compulsive disorder, and autism. Furthering the development of effective treatments for individuals with these disorders requires a more comprehensive understanding of the physiological processes mediating

behavioral adaptability. The overarching aim of this project is to develop a novel experimental paradigm to explore the detailed neurophysiological substrates of cognitive flexibility using the laboratory rat as an experimental model.

Anticipated Duration of Project

1/1/2010 - 12/31/2012

Project Overview

Our general aim is to investigate the neurophysiological substrates underlying the ability of rats to flexibly adapt their behavioral strategy in an effort to acquire rewards. Our hope is that knowledge gained from this project will facilitate the further development of pharmacological and behavioral interventions aimed at treating disorders that compromise cognitive flexibility, such as schizophrenia, obsessive compulsive disorder, and autism.

Current evidence suggests that the prefrontal cortex and striatum work in concert to flexibly guide behavioral output toward adaptive ends. We will record single neuron activity from these two regions in awake, behaving rats as they employ multiple strategies in a visual discrimination task for rewards. In our first aim, we will train rats to discriminate between two visual patterns, each presented to either the right or left side. Subjects will be required to indicate the location of the target of interest by releasing one of two response levers with one of their forelimbs. Our second aim is to extend this paradigm to investigate the neural correlates of attentional set-switching, the ability to select and focus on a subset of available sensory information to guide behavioral decisions. This will constitute a test of cognitive flexibility which has been shown to be influenced by medial prefrontal cortex. Ultimately, our goal is to successively introduce two additional attributes to the visual patterns: luminance (normal or bright) and visual stability, where each pattern will either remain steady or flicker. Subjects will be trained to empirically identify and selectively attend to the one of the three stimulus dimensions which is relevant to obtaining reward (ex., releasing the lever corresponding to the appropriate pattern, while ignoring differences in luminance and stability). For the period covered under the present funding, we plan to begin training subjects on one additional dimension: luminance.

Prefrontal cortex is thought to encode behavioral rules relevant to achieving goals, while neurons in the striatum are known to respond to goal-directed forelimb movements and to sensory stimuli that elicit these movements in trained animals. We will study the neuronal activity underlying the ability to alter behavioral strategies to achieve goals as external environmental demands (task rules) change. We hope these studies will lead to a better understanding of how neurons in the prefrontal cortex and striatum reorganize their activity to accommodate changes in task requirements.

Principal Investigator

Jeffrey T. Oristaglio, PhD
Research Assistant Professor
Department of Pharmacology and Physiology

Drexel University College of Medicine
245 N. 15th St.
Philadelphia, PA 19102

Other Participating Researchers

Jed S. Shumsky, PhD - employed by Drexel University College of Medicine

Expected Research Outcomes and Benefits

Severe rigidities in both thoughts and actions result from a variety of neurodevelopmental and psychiatric disorders. Such behavioral abnormalities are debilitating to the afflicted individual, often stunting the development of social interactions and language skills. For family members and caregivers, they are often a source of frustration and hardship, and can ultimately present a significant impediment to the effective treatment of the underlying disorder. The goal of this project is to better understand how the brain mediates the flexibly adaptive goal-directed behavior which is characteristic of normally-functioning individuals. Particularly, we wish to understand how the brain modifies behavioral strategies to respond to changing environmental circumstances, and how these strategies are used to formulate appropriate goal-directed behaviors. We will develop a series of novel studies to investigate the neurophysiological substrates of cognitive flexibility in rats trained to selectively attend to changing stimulus-response contingencies on a reward-based visual discrimination task. The proposed studies are timely, as new and potentially useful rat models of neuropsychiatric disorders such as Obsessive-Compulsive Disorder, Attention Deficit Disorder, and Autism are being developed and tested. A thorough characterization of the differences in brain activity underlying properly adaptive and cognitively rigid behaviors will provide a biomarker with which to assess the likely efficacy of putative therapeutic compounds. If realized, our project objectives will productively extend the investigative options of researchers interested in studying important aspects of executive function, thus facilitating the further development of ongoing translational research aimed at developing treatments for neuropsychiatric and developmental disorders.

Summary of Research Completed

The overarching goal of this project was to explore the physiological substrates of cognitive flexibility: the capacity of animals to alter their behavior in response to changing environmental challenges. We proposed to approach this problem by training water-deprived rats to perform complex, rule-based visual discrimination tasks in which the strategy required for gaining rewards is changed without warning. While we made some progress toward achieving our goals for Aim 1, we encountered a number of impediments. Our first implanted subject dislodged his implant while undergoing acclimation training to head fixation following completion of the first stage of task training. We were forced to temporarily withdraw this subject from testing. This subject subsequently developed an abdominal tumor and had to be removed from the study prior to performing recordings. We have improved upon our initial implant technique by adjusting the number and type of bone screws used to attach and anchor the implant to the skull. Our newer implants have met with much better success and have proved to be stable over several months and have not adversely affected the health of subjects in any way.

We also discovered that adaptation to head fixation is best done prior to, and parallel with, training on behavioral tasks. Subjects that do not undergo surgery and head fixation training prior to task training have not fared well in our pilot studies. We have now adopted the procedure of performing the surgical implantation procedure and training on head fixation *prior* to task training. Although this requires additional time for performing maintenance on the recording chambers (regularly cleaning them to prevent infection), our subjects have fared much better in adapting to this progression.

Finally, training on the original proposed tasks has proven difficult for our rats, and, if at all possible, does not appear to be feasible within the timeframe we expected. Our overarching goal was to have subjects perform an attentional set-shifting task in the head-fixed condition (Aim 2). To achieve this, we set an intermediate goal for Aim 1, in which we proposed to train subjects to perform a visuo-spatial mapping task where they first press two levers with their forepaws and release the lever corresponding to the side of space at which a visual stimulus appears. We achieved this goal for 2 of the 3 initial subjects we trained for this study, and this was detailed in our previous progress report. The third rat had a strong right paw dominance which resulted in repeated premature and incorrect responses with that paw (release of right lever for stimulus on the left side). We were unable to train this subject out of these tendencies and he never progressed past the early, experimenter-controlled training phase.

Early attempts to transition subjects from the visuospatial recognition task to the pattern discrimination task (2nd portion of Aim 1) did not meet with success. This prompted us to define a new task for assessing cognitive flexibility. We attempted first to train subjects to reverse the original stimulus-response mapping; to lift the left paw in response to a light appearing on the right side of space and vice versa. One of the two subjects was able to adapt to this rule change but was extremely slow to learn it, and required multiple sessions to reach a criterion level of performance (roughly 75% correct trials). Furthermore, further training did not improve the time it took him to switch rules, making it unlikely that we would achieve one of our original goals of recording the same set of single neurons while subjects perform a rule switch. The other subject had a strong paw preference that he could not be trained to overcome when attempting to perform this stimulus-response reversal. This subject was trained to switch his strategy to releasing the left lever (dominant paw) regardless of stimulus location (egocentric rule) but never achieved a consistent level of performance comparable to that seen with the original rule.

The amount of time it took to train subjects to perform the original task and rule-switches (approximately 4 months) and the projected attrition due to subjects unable to perform these tasks (one of our three subjects), cast doubt on the viability of the project as originally conceived. These problems forced us to reevaluate our task design. Our goal was to create a new task that could ultimately be used to achieve our initial goal of exploring cognitive flexibility while satisfying a number of additional constraints. First, we sought to shorten the duration of time required to train subjects on a task. This included eliminating the problem of preference for the dominant paw which interfered with learning and forced inconsistencies in the way subjects were trained to perform the task. Second, we reduced task complexity by requiring subjects to attend to only one visual object at a time. Because rats are inherently impulsive and distractible, effectively constraining spatial-attention requirements to one location would likely make the task

more easily understandable, and result in faster training. Additionally, we wanted a task that could be taught in multiple stages of progressive complexity, with each stage providing useful behavioral data to be combined with electrophysiological measurements. This would help to ensure that most, if not all, of the subjects that completed head-fixation would be capable of contributing at least some data on both task performance and neuronal activity. Finally, we wished to maintain the original requirement that subjects release a lever to signal a behavioral decision, thus satisfying our original goal of providing an accurate measure of reaction time.

Simplified task design and additional experimental aims

Currently we have trained 3 subjects to perform a visual signal detection task in the head-fixed condition. This new task will also allow us pursue new goals of examining the physiological processes underlying sensory detection and sustained attention, while providing a platform for more complex tasks assessing cognitive flexibility. In this task, subjects depress a small response lever with one paw to initiate a trial. On most trials, after a variable time delay, a visual stimulus (a circular white spot, 8 cm in diameter) appears in the center of a video screen located approximately 26 cm in front of the subject's eyes. Subjects release the lever to indicate detection of the stimulus and receive a small drink of water. On 25-30% of the trials no stimulus is presented and subjects are required to hold the lever for 1500 ms (the shortest pre-stimulus delay used during testing). Task difficulty is varied by controlling stimulus luminance which can be made arbitrarily low. Once trained, subjects undergo two types of testing: random and block testing. In random testing, one of three stimuli of varying luminance is selected randomly on each trial. In block testing, subjects are presented with stimuli of a constant luminance in blocks of 100 or more trials. Subjects begin a session with either the easiest (highest luminance) or most difficult (lowest luminance) stimulus (randomly chosen), and are then switched to the other. Random testing will be used to measure the average responses of medial prefrontal cortex neurons to stimuli of varying detectability. Block testing allows for comparisons of neural activity during periods of high and low task proficiency while stimulus intensity remains constant. This is important as we have found that even well-trained rats perform variably throughout a single session, progressing through periods of proficient and poor performance. The nature of this change is clearly not related to stimulus energy or task difficulty, and we are interested in the mechanisms underlying this effect. Conversely, block testing also provides for an analysis of how medial prefrontal activity changes in response to stimulus luminance changes during periods of good performance.

This additional focus will be relevant to understanding the mechanisms of Attentional Deficit Hyperactivity Disorder (ADHD) and for providing additional assays for novel, putative therapeutic compounds designed to treat this disorder. We are now collaborating with the laboratory of Dr. Barry Waterhouse in the Department of Neurobiology and Anatomy at the Drexel University College of Medicine to pursue these additional experimental avenues.

Our goal is to use this newly-conceived Aim 1 as a foundation for training subjects on visual discrimination tasks, where they will differentiate between two different stimuli by releasing for one and holding for the other. This general task design is similar to one used in the studies of Rajkowski and colleagues (2004) who investigated visual discriminations in monkeys. These investigators were able to extend this technique to train subjects to perform stimulus-response

reversals, a simple test of cognitive flexibility. This new task progression will also allow us to measure differences in how visually-sensitive mPFC neurons represent simple object detection in comparison to discriminations where the shape of the object must also be evaluated. This is an important goal which was not accounted for in our original experimental design.

Single-neuron, multi-unit and local field potential recordings from awake, behaving, head-fixed rats

We have made significant progress toward realizing these newly-defined goals. We have trained 3 subjects to perform the visual detection task, and a fourth subject is undergoing head fixation training. Figure 1 displays representative performance on this task from three subjects (A-C) during single testing sessions. The left panel displays percent 'hits' (correct detections) divided by the number of hits and 'misses' (failures to respond when a stimulus appears). As can be seen, detection rate is generally lower for low-luminance stimuli. Furthermore, lower detection rates are accompanied by slower reaction times. This general psychophysical relationship has been reported with variations in difficulty in many different tasks and provides an important validation of our technique.

To date, we have recorded a total of 72 single neurons from 3 subjects (24 from subject 1, 8 from subject 2, and 40 from subject 3) in both hemispheres of the medial prefrontal cortex (mPFC). Additionally, we have recorded local field potential (LFP) activity and multi-unit activity (in cases where neurons with smaller signals cannot be individually isolated, or when there are more single-neurons than can be isolated with our online spike sorting system). We have sampled a range of locations along the anterior-posterior axis of the mPFC (anterior 1.0-2.8, relative to Bregma). Thus far, we have discovered that some mPFC neurons exhibit visually-evoked activity that differentiates between hits (correct detections of the stimulus) and misses, failures to respond when a stimulus appears (Figures 2 and 3). An additional, surprising finding is that the LFP signal at the beginning of a trial, prior to stimulus presentation, exhibits higher relative amplitude in the theta and alpha frequency ranges when subjects respond impulsively by releasing the lever prior to stimulus presentation (Figures 4 and 5).

A portion of this preliminary data has been included as part of a collaborative R21 grant proposal (with the laboratory of Dr. Barry Waterhouse) to the National Institute for Child Health and Human Development. We have proposed to use the head-fixed signal detection task to study the effects of methylphenidate on early visual sensory processing and sustained attention.

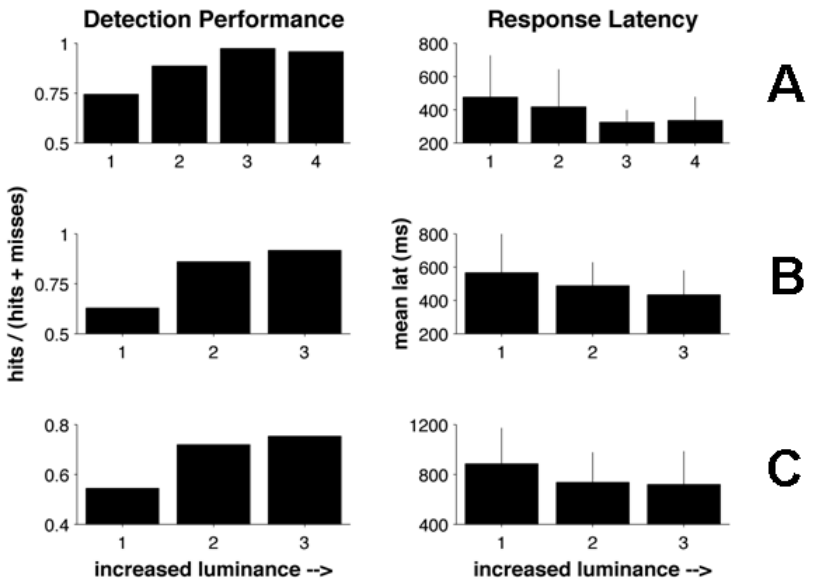

Figure 1. Representative detection performance and response latencies from single testing sessions on 3 subjects (A-C) performing the visual detection task. Stimuli were circular white patches (8.4 cm diameter) presented on computer video monitor 26 cm in front of the subject. In general, detection performance declines and response latencies increase as stimulus luminance is decreased. This is consistent with an increase in task difficulty. The subject in (A) was tested with 4 different luminances while subjects in (B) and (C) were tested with 3.

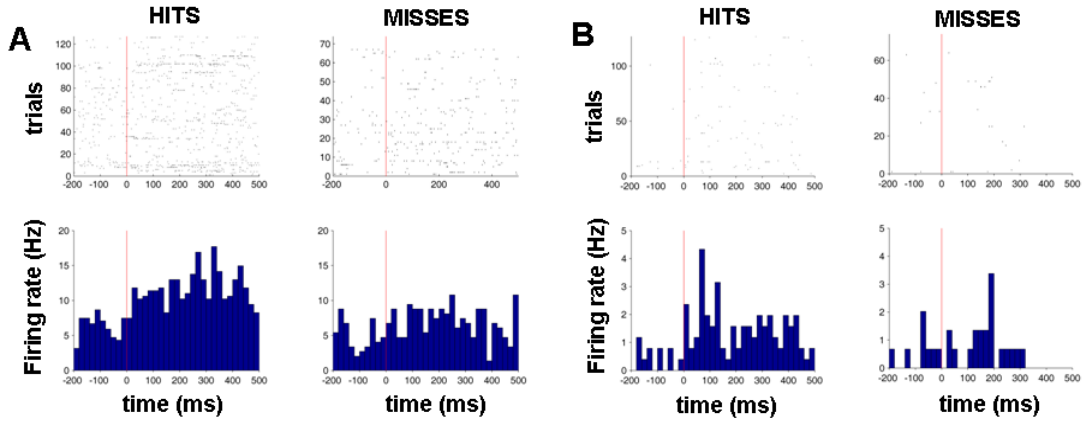

Figure 2. Visually-evoked responses for hit and miss trials from a single subject performing the visual detection task. (A) Multiunit activity. (B) Single neuron recorded in the same session. Raster plots (top row) display action potentials recorded over time. Rasters are aligned with onset of the visual stimulus (red line), which appeared for 250 ms. Bottom row plots display corresponding mean spike rate histograms (bin width=20ms). Notice that the average activity for hits (correct detections) is more robust both in the baseline period (prior to stimulus onset) and after stimulus onset.

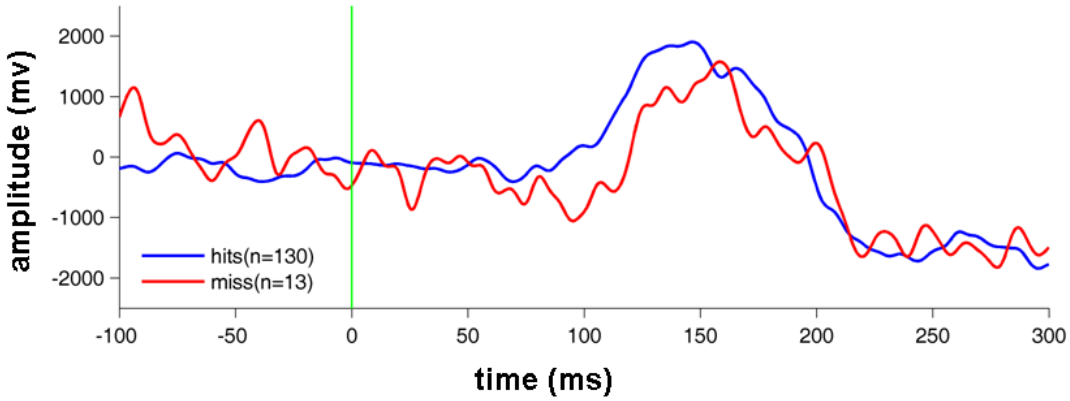

Figure 3. Visually-evoked local field potential (LFP) activity on hit and miss trials. Consistent with single and multi-neuron data (Figure 2), LFP activity also shows reduction during miss trials. The effect shown here did not reach statistical significance, though this may be due to the small number of miss trials. We are in the process of examining these differences across sessions and in different subjects to see if this pattern is repeated. (Local field potential activity was filtered at 1-100 Hz. Signals are smoothed with a gaussian kernel, width = 24 std dev).

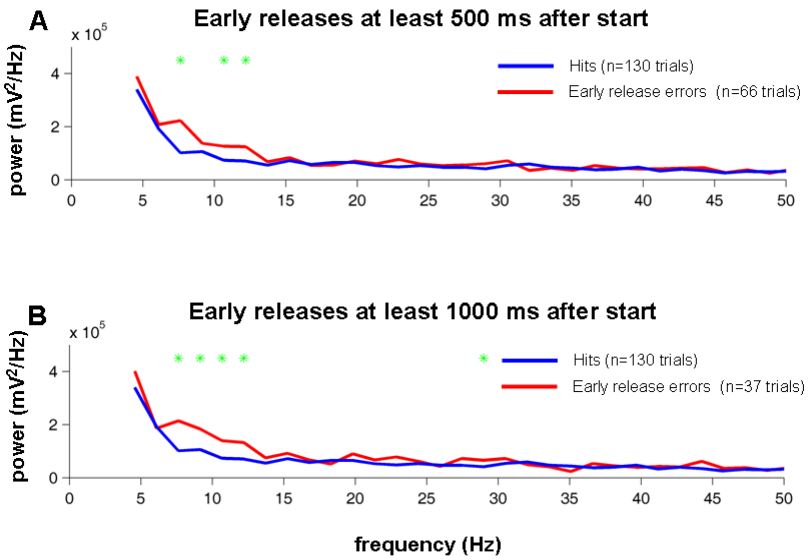

Figure 4. Comparison of power spectrum for medial prefrontal cortex LFP signal on trials with correct detections (hits) and early release errors (releases prior to stimulus presentation). Plots display the median power across frequencies of 5-50 Hz for hits and early release trials, where the subject released the lever prior to stimulus presentation. Power spectra were calculated for the first 500 ms of the trial. (A) Early release analysis was restricted to trials where the premature release occurred at any time point 500 ms after the start of the trial. Early release trials, a reflection of impulsive behavior, are associated with increased power in the mid-high theta (3-8 Hz) and alpha frequency (9-14 Hz) ranges. (B) The same analysis repeated for early releases occuring at least 1000 ms after the start of the trial (at least 500 ms after the end of the analysis window). Notice that the effect is actually more pronounced when the temporal separation between the analysis window and the time of response is increased. This suggests that the increased power in early release trials is not simply a reflection of pre-motor activity, since such

activity would be more pronounced near the time of release. (LFP signals were analyzed with Matlab's discrete fast fourier transform. Green asterisks indicate significant differences for respective frequency, $p<0.05$, Kruskal-Wallis ANOVA).

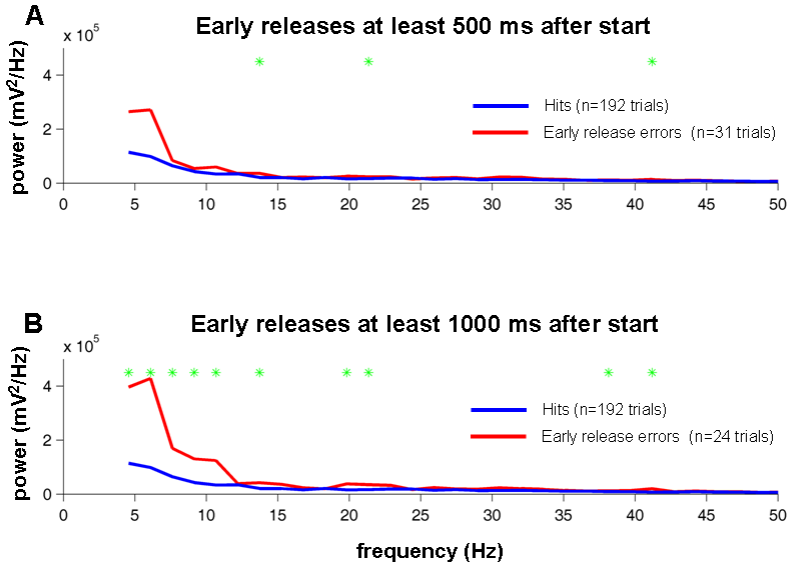

Figure 5. Power spectrum for medial prefrontal cortex LFP signal for on hit and early release error trials. Early release errors in this subject are accompanied by higher power in the lower theta as well as the alpha range. Conventions and analysis as described in Figure 4.

Research Project 9: Project Title and Purpose

Microfabricated QLISA Biosensor with Embedded Heating and Mixing Elements – The purpose of this project is to develop a novel, low cost microfabricated poly (methyl methacrylate) (PMMA) Quantum-dot-Linked-ImmunoSorbent-Assay (QLISA) biosensor with embedded mixing elements. The significant advantages of this microfluidic platform with integrated electrokinetic mixing are: *a)* Higher optical detection sensitivity *b)* Improved detection limit *c)* Higher signal to noise ratio *d)* Reduction of assay *e)* Multiuse system - repeated use of the sensor is possible, and *f)* Platform technology – can be used to detect any biomarker. The bioassay platform developed will use only 1-2 microliters of sample and achieve detection sensitivity of picomolar quantities of antigen.

Duration of Project

1/1/2010 - 6/30/2011

Project Overview

The broad research objective of this project is to develop a novel, low-cost all plastic microfabricated biosensor with embedded mixing elements. *The specific research aims* are 1) Design, fabrication, and testing of a polymethyl methacrylate (PMMA) microchannel for Quantum-dot-Linked-ImmunoSorbent-Assay (QLISA), 2) Enhanced sensitivity by physical and

chemical modification of the channels, and 3) Incorporation of electrokinetic mixing onto the PMMA microchannel.

Aim 1: Design, fabrication, and testing of a PMMA microchannel for QLISA
Rectangular microchannels with a width of 100-300 μm, a depth of 10-50 μm, and a length of 2 mm will be fabricated on thin (1-2 mm) PMMA substrates by hot embossing. The substrates will then be bonded via thermal fusion bonding to flat PMMA substrates that have been machined to have inlet and outlet holes. Carboxyl groups (COOH) required for immobilizing antibodies will be induced on PMMA chips via UV assisted selected area functionalization.

Aim 2: Enhanced sensitivity by physical and chemical modification of channels
Physical modification: Excimer laser (ArF, 193 nm) ablation will be used to create diverse microstructures (grooves, pillars, grids, wavy surfaces, etc.) on the bottom of the PMMA microchannels. *Chemical modification:* PEI, a cationic amine-bearing polymer, will be used to chemically modify the PMMA channel surface. These modified PMMA microchannels will be directly used for immobilizing antibodies specific to Myeloperoxidase (MPO).

Aim 3: Incorporation of electrokinetic mixing onto the PMMA microchannel
Among several electrokinetic mixing techniques the electrothermal effect has been identified as the optimal approach for the current application. Rotational flow patterns due to electrothermal effect will be achieved via interdigitated gold microelectrodes in the PMMA microchannel. These planar microelectrodes will be fabricated on flat PMMA substrates using the lift-off technique. The rotational flow can be observed under a microscope via the motion of microbeads suspended in the solution. Finally, the effect of electrothermal mixing on the sensor performance will be evaluated through actual QLISA assays for MPO.

Principal Investigator

Elisabeth S. Papazoglou, PhD
Assistant Professor
Drexel University
School of Biomedical Engineering
3141 Chestnut Street
Philadelphia, PA 19104

Other Participating Researchers

Hongseok (Moses) Noh, PhD, Sundar Babu Nadarajan, PhD – employed by Drexel University
Sreekant Murthy, PhD – employed by Drexel University College of Medicine

Expected Research Outcomes and Benefits

The project will develop a sensitive cost effective immunoassay as a platform technology for adoption into many health care fields. The biomarker chosen to validate the technology is a ubiquitous inflammatory marker present in heart disease and in many auto-immune disorders. Health status will be improved because tests can be run on small samples, faster and more

economically. The applications for this technology include public health emergencies where a point of care fast test is critical to assess the effect of a biohazard or an infectious disease in the population. Neonate care where sample size is critical can benefit from a test that can give an answer with 1 to 5 microliters of a sample.

The proposed research emphasizes collaboration and development of junior faculty. It will lead to increasing the number of new investigators and by developing stronger grant applications the number of funded grants awarded to the State of Pennsylvania. New products will be developed that can attract new companies to be formed to further commercialize the technology. Since QLISA has been originally funded by the Coulter foundation, business and community involvement is present and can be seamlessly transferred to the innovations developed in the proposed grant.

Summary of Research Completed

This study completed a quantum dots based microchannel fluorescent immunosensor with embedded AC electrokinetic mixing elements. Microchannels were fabricated on inexpensive commercially available poly methylmethacrylate (PMMA) sheets by using a solvent-based polymer imprinting and binding method. A low cost UV-LED was used as an excitation source, and data were collected by a CCD camera. The results indicate that the microchannel device with the specific optical setup is capable of detecting myeloperoxidase (MPO) at a sensitivity limit of 0.6 nM. In order to achieve faster detection, electrothermal flow was integrated into the microchannel device as an active mixing element, and driven at a frequency of f = 200kHz and 6 Vrms. The electrothermal enhancement of the assay demonstrates the ability of electrothermal mixing to reduce the assay time significantly.

Quantum dots (QDs) have gained widespread recognition due to their unique optical properties such as broad excitation wavelengths, narrow emission spectrum, and photostability. The surface of quantum dots can be modified for different biological/chemical applications. Polymer coating modification has shown advantages that are superior to phase transfer by ligand exchange in many aspects.

In this report we present a microfabricated quantum dot linked diagnostic assay (QLIDA) biosensor with an embedded mixing element. *Our selection of PMMA was based on its optical properties and capability to selectively functionalize its surface for antibody immobilization.* Microchannels were fabricated by using a fast, solvent-based polymer imprinting method. Microchannel dimensions of 100 μm deep, 250 μm wide, and 2.5 cm long allow us to use a volume less than 2 μl. The microchannel is easy to fabricate on PMMA sheets, and less expensive than a PMMA capillary. With an active mixing element, the detection time was significantly reduced from about 3.5 hours to 30 minutes. The inexpensive device described below was used for detecting myeloperoxidase (MPO) and measuring its concentration. MPO is an inflammatory marker over-expressed in inflammatory diseases. Our initial results indicate that it is possible to develop a low cost, fast detection immunofluorescence sensor capable of operating with ~2 μl of analyte and detecting nanomolar concentrations of MPO.

Velocity: numerical model and experiment observation
The particle (polystyrene bead) movement due to ETF was observed as the amplitude and frequency of the applied voltage was varied. At a high frequency (200kHz) condition, ACEO does not exist, while ETF is dominant in this condition. Below $3V_{rms}$ no particle motion was observed. As the voltage was increased, particles became more and more active until the electrodes were damaged at $10V_{rms}$. The experimental results had a good agreement with the numerical simulation shown in Figure 3. For immunoassay, a large scale and mild fluidic hydrodynamic motion is desired. Thus, a set of parameters ($6V_{rms}$, 200kHz) was chosen for immunoassay experiments.

Optimization of optical detection system
As shown in Figure 2, the optical setup is comprised of a firewire monochrome CCD camera (Stingray, AVT-FS-033B), a UV-LED rated at 27 mW optical power, an excitation filter was used to cut off other but desirable excitation light and another bandpass filter (600±20) was mounted on the detection side to remove any interfering signal, an aspheric lens served the purpose of concentrating the UV light to a spot size of ~1.5 mm. The angle between the UV source and CCD camera was maintained at 60º. A serial dilution of QD 605 streptavidin was prepared to test the sensitivity of the optical detection system, and it was repeated three times. In order to generate high power of the UV source while protect the LED from burning down, the power supply constantly offered 5 V, 0.5 Amp power to the UV-LED. Different camera shutter speeds and gains were tested to improve the performance of the optical setup. It was found, as shown in Figure 4, a linear relationship between the concentrations of QD solutions and the fluorescence intensity can be obtained at a shutter speed of 890 ms and 50% gain. It was also found that at such parameters setting, the camera reached saturation with 5nM of QD 605 streptavidin.

All PMMA assay
Immunoassay was carried out based on a typical pAb/MPO/QD-mAb sandwich assay. In all the immunoassay, 10nM of QD 605 streptavidin was used. The concentration is far more than enough (5 nM) to saturate the camera. QD streptavidin conjugate could be conjugated with biotin-mAb complex beforehand. However, this additional step may cause the loss of a mount of antibody as well as QD during the separation of QD-mAb complex from QD and antibody.

BMP image data collected from the CCD were analyzed and resulted in quantification of the concentration of MPO based on the fluorescence intensity of the QD. A region of interest (ROI), typically 15×40, was chosen at the geometrical center of the microchannel. An average of the intensities of all the pixels within the ROI was obtained using ImageJ.

Though the dominant binding mode is one QD streptavidin conjugate per analyte, it should be noticed that there are typically 5-10 streptavidins covalently attached on the surface of each quantum dot according to the protocol provided Invitrigen. When the concentration of the analyte, MPO in this case, is low, QD streptavidin conjugate react with biotin-mAb by 1:1 ratio. However, when the concentration of MPO exceeds the saturating concentration, it is predictable that one QD may bind to more than one MPO-mAb complex, resulting in artificially reduced signals. This assumption is fit with the experimental result. In Figure 5, there is a clear signal

intensity drop, which indicates that given the concentration of QD, the MPO-mAb complex reached the saturation concentration at 20nM.

Si/PMMA assay

The imaged results are shown in Figure 6. Figure 6(a) shows a typical control case assay that was performed with no electrothermal mixing and allowed to react for 5 min. Figure 6(b) is a typical 5 min reaction assay that was enhanced with the electrothermal mixing. The electrodes were energized with an applied potential of $6V_{rms}$ and a frequency of f = 200kHz for 5 min. The fluorescent spot is brighter, which indicates improved binding and a faster reaction. The images were taken from near the mixing electrodes area rather directly from the electrodes area, due to the fact that reflection from the gold electrodes interfered the detection by increasing the background signal.

Quantification of the image data was achieved through fluorescent intensity measurements using ImageJ. The results are shown in Figure 6. Without ETF mixing, the fluorescent signal was very low, indicating that there is limited binding between pAb and MPO, and between MPO and QD-mAb within 5 minutes. However, with ETF mixing, the binding efficiency was greatly improved, and signal intensity was comparable to the normal MPO assay with 1 hour incubations.

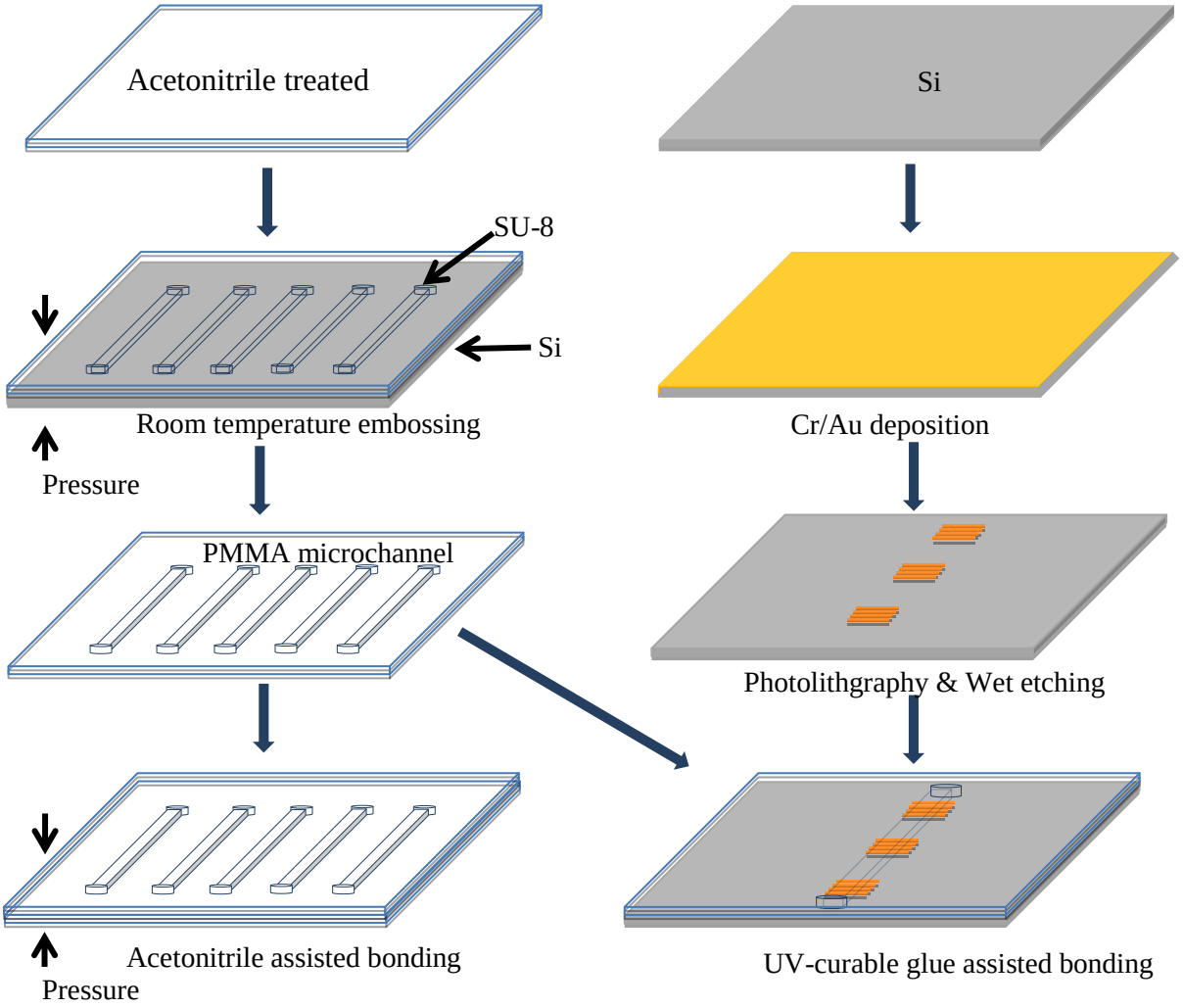

(a)

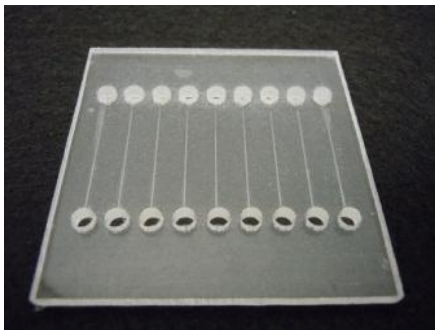

(b)

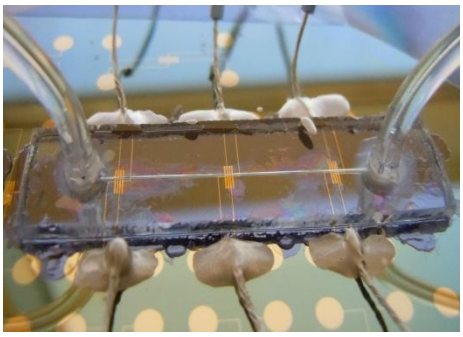

(c)

Figure 1. (a) Schematic of fabrication process. Microchannel fabrication and all PMMA device bonding are achieved with the assistance of acetonitrile. Bonding between PMMA and Si is assisted by UV-curable glue. (b) All PMMA microfluidic device. (c) Si/PMMA microfluidic device.

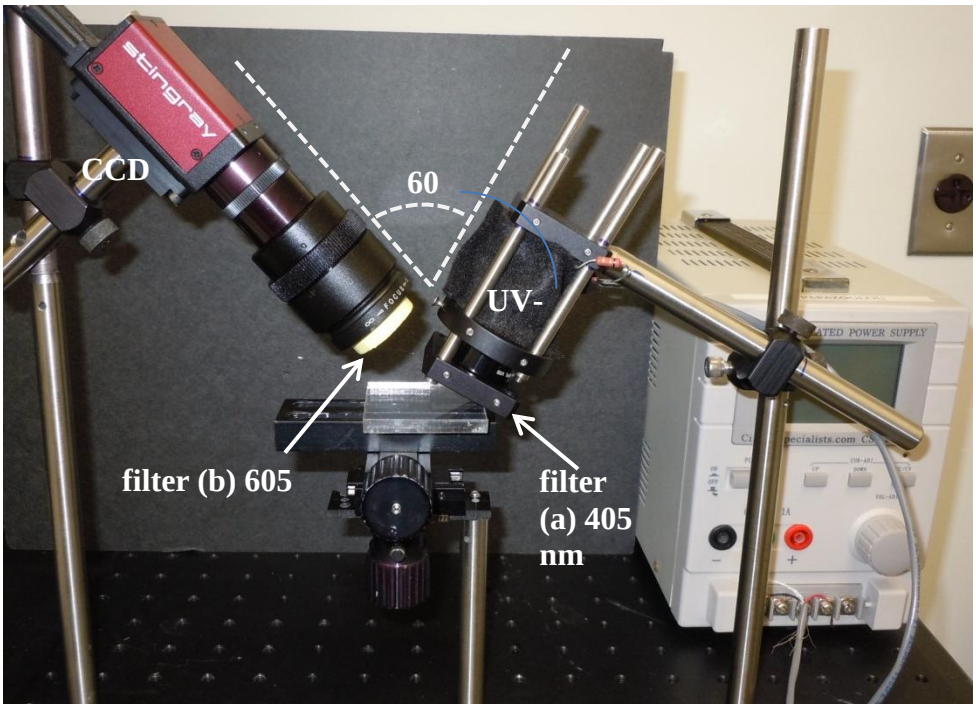

Figure 2. Optical setup for fluorescence signal collection from quantum dots.

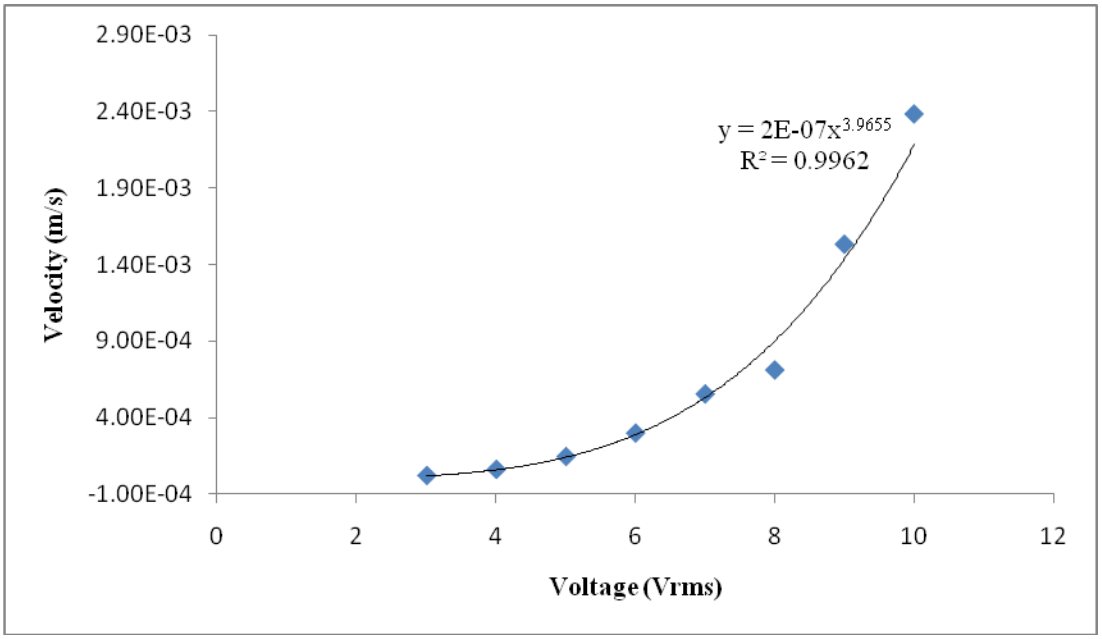

Figure 3. Numerical simulation result of fluid velocity as a function of the applied voltage. Frequency was fixed at 200kHz. At 6 Vrms, the velocity is 296 μm/s.

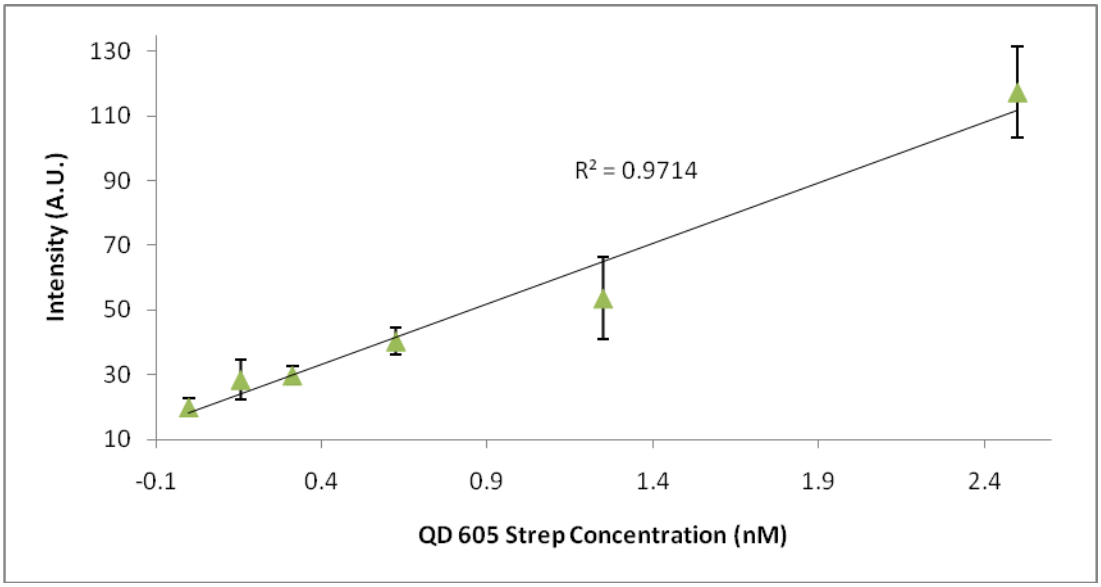

Figure 4. QD 605 Streptavidin calibration curve. A linear, high signal to noise ratio curve was obtained at shutter speed of 890 ms, 50% gain. Signals, not shown here, from 5 nM QD saturate the camera at given parameters setting.

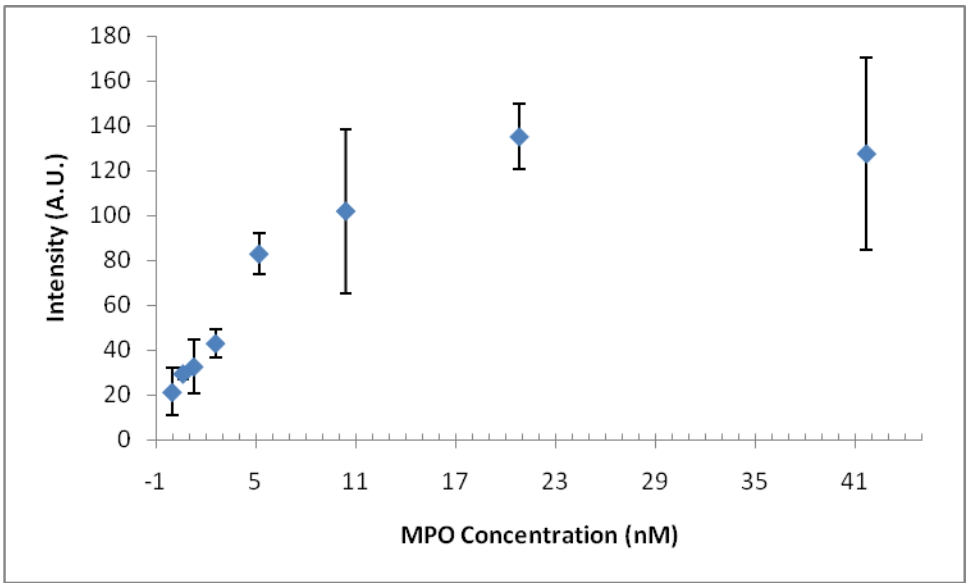

Figure 5. Calibration curve for the sandwich QLIDA in all PMMA microfluidic device. The data points are the average of three independent measurements performed with three different microchannel devices.

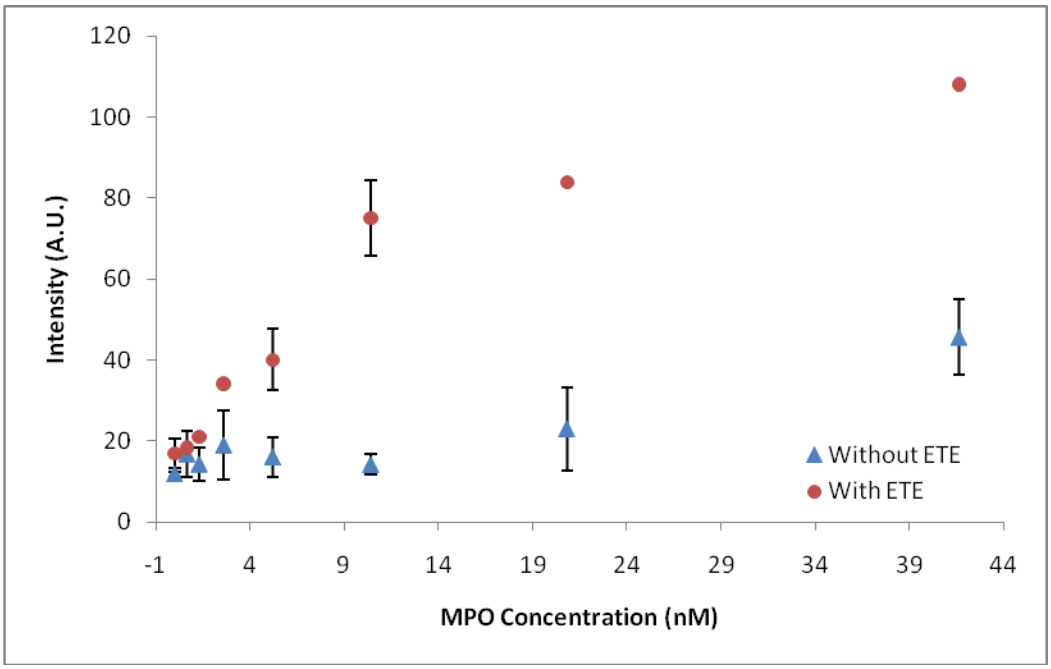

(a)

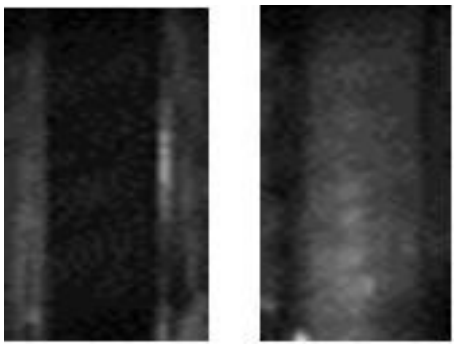

(b)

Figure 6. QLIDA assay intensity with and without electrothermal flow (ETF) mixing. (a) Significant increase in the intensity is observed with ETF mixing. (b) Results with ETF mixing (left), and result without ETF mixing (right).

Research Project 10: Project Title and Purpose

The Role of miRNAs in Modulating Alzheimer's Disease Risk - We will test the hypothesis that genetic variation in the 3' untranslated region (3'UTR) of the human amyloid precursor protein (APP) gene may modulate the risk of developing Alzheimer's disease by disrupting miRNA mediated regulation APP levels. The genetic basis of Alzheimer's disease (AD) is not fully understood. Identifying polymorphisms that increase risk will allow for early prediction of who may develop disease. This knowledge may also lead to a novel therapeutic approach to treating AD with molecules that act like miRNAs to decrease APP levels.

Anticipated Duration of Project

1/1/2010 - 12/31/2012

Project Overview

In the past decade our view of RNA has changed dramatically with discovery of non-coding RNAs that regulate gene expression. In particular, microRNAs (miRNAs) function to post-transcriptionally regulate gene expression. miRNAs are RNA molecules 21-23 nucleotides in length that bind to the 3' untranslated region (3'UTR) of messenger RNAs (mRNAs) that have sequences complementary to the miRNA. miRNA binding to this target sequence inhibits translation of the specific mRNA. miRNAs are endogenous negative regulators of gene expression. This function leads miRNAs to be important and even essential regulators of normal cell homeostasis, organismal development, and human diseases. Approximately 800 miRNA genes have been identified in the human genome with a large percentage of these expressed in the human brain.

Emerging evidence suggests that miRNAs may play a role in Alzheimer's disease (AD). The precise mechanisms that cause AD are not completely understood, however proteolytic processing of the amyloid precursor protein (APP) to generate the β-amyloid peptide (Aβ) seems to play a fundamental role in disease pathogenesis. APP is sequentially cleaved by the β- and γ-secretases to generate Aβ, which is known to lead to synaptic dysfunction and give rise to deficits in learning and memory. In AD patients, brain miRNA expression is altered compared to normal aged controls. We recently reported that miR-106a and -520c can regulate APP protein levels. DeStrooper and colleagues then demonstrated that miR-20a, -17-5p, and -106b could also regulate APP levels. Given that trisomy 21 (the human *APP* gene is located on chromosome 21) or *APP* locus duplication are sufficient to cause AD, this suggests that disruption of the miRNA mediated APP regulation may lead to AD.

To test the hypothesis that genetic variation in the 3' UTR of the human APP gene may modulate the risk of developing Alzheimer's disease by disrupting miRNA mediated regulation APP levels, we will (i) identify common polymorphisms in the APP 3'UTR, (ii) test the effect of these polymorphisms on miRNA-mediated regulation, and (iii) determine if these polymorphisms are over-represented in AD patients versus normal, aged controls.

Principal Investigator

Aleister J Saunders, PhD
Associate Professor
Drexel University
3141 Chestnut Street
Stratton Hall
Philadelphia, PA 19104

Participating Researchers

Carol Lippa, MD, Andi Russo, Neha Patel - employed by Drexel University

Expected Research Outcomes and Benefits

The results from this project's experiments will allow us to determine if common genetic variation found in the 3' untranslated region of the human APP gene results in modulation of miRNA mediated regulation of APP levels. This is important since this may reveal a heretofore unappreciated route to developing AD. This would allow for early prediction of individuals that would develop disease, something that is missing for all but the most extreme cases. In addition, the identification of a new mechanism that leads to the development of Alzheimer's disease may also allow for the identification of new approaches for therapeutic intervention.

Summary of Research Completed

Overall the Commonwealth funding has been crucial in obtaining compelling preliminary data. We will be utilizing this data for an Oct. submission of an NIH R01 proposal.

The hypothesis that we tested is that genetic variation in the 3' UTR of the human *APP* gene may modulate the risk of developing Alzheimer's disease (AD) by disrupting miRNA mediated regulation APP levels. This disruption would cause an increase in APP levels, which is a known cause of AD. To test this hypothesis we proposed three aims: (i) identify common polymorphisms in the *APP* 3'UTR, (ii) test the effect of these polymorphisms on miRNA-mediated regulation, and (iii) determine if these polymorphisms are over-represented in AD patients versus normal, aged controls. Below we detail the results we have obtained during this reporting period.

<u>Aim 1: Identify common polymorphisms in the human *APP* 3'UTR.</u> As we described in our initial progress report, we utilized two experimental approaches to identify genetic variation in the 3'UTR of *APP*; direct sequencing of select patients and bioinformatics based polymorphism identification. These efforts lead to the identification of three single nucleotide polymorphisms, rs45455403, rs45541739 and rs1059478. As noted last year, rs45455403 and rs45541739, are found predominantly in individuals who identify themselves as African Americans. This past year we extended our polymorphism discovery efforts by directly sequencing the APP 3'UTR of 110 African American (AA) individuals recruited as part of this project. This is important because our initial sequencing efforts were in predominantly Caucasian families. We have identified four novel, rare mutations (Table 1). None of these novel polymorphisms were found in more than three subjects. Two of these are located in regions in predicted miRNA target sites. We are currently working to determine if these polymorphisms have functional effects on miRNA gene expression regulation (Aim 2).

<u>Aim 2: Test the effect of these polymorphisms on miRNA-mediated regulation.</u> In our last progress report we detailed our results that provide evidence that the minor allele of rs45455403 disrupts miR-495 mediated regulation of APP expression. A manuscript describing this work has been written and is now undergoing final edits prior to submission.

In the year since we've submitted our initial progress report, we focused on determining if rs45541739 and rs1059478 affect miRNA mediated regulation of APP using the same experimental approached used for testing rs45455403. Our results suggest that neither miR-29 nor miR-376 affect APP expression and that the polymorphisms do not alter this (data not shown).

We have demonstrated allele specific disruption of miR-495 mediated regulation of APP expression. This suggests a novel pathogenic mechanism for AD whereby disruption of miRNA/APP mRNA interaction would lead to increased APP levels and eventually AD. We have concluded that rs45541739 and rs1059478 do not affect miR mediated APP expression. We are now investigating if the novel polymorphisms identified in Aim 1 alter miR mediated APP expression.

Aim 3: Determine if polymorphisms found in the predicted miRNA target sites of *APP* are over-represented in AD patients versus normal, aged controls. Given the strong functional data in Aim 2 we set out to determine if rs45455403 was over-represented in AD patients compared to controls. rs45455403 is found almost exclusively in the African American community. Since African American AD research cohorts are rare, we are recruiting patients in the Drexel University Memory Disorders clinic who identify themselves as African American. As controls we recruit unaffected family members. We have recruited 111 subjects to date, a summary of affection status is shown in Table 2. Given the increased risk of developing AD in the AA population and the paucity of AD research cohorts that contain significant numbers of African Americans the establishment of this research cohort is an important development in our efforts to understand the basis for the increased AD risk in this population. We are continuing to recruit subject and controls. Also given the emphasis at NIH on understanding differential disease risk in under-represented populations we feel our upcoming NIH submission will be viewed positively.

Our analysis has revealed that individuals carrying the minor allele of rs45455403 are not solely AD patients. In fact the polymorphism is equally represented in affected and unaffected individuals. While these findings disprove our hypothesis we believe that this polymorphism might still contribute to AD risk. The vast majority of genetic risk factors for late onset AD have very small effects, that is they are found in both affected and unaffected individuals. To definitively determine if these polymorphisms have an effect on very large numbers of unaffected and affected individuals (e.g., 10,000) will be required. It is also possible that other "private" mutations that target APP miRNA target sites exist and may affect risk. The novel polymorphisms discovered here could be such "private" mutations. Our future work will test this hypothesis.

Table 1. Novel polymorphisms

	Sequence Context
1	ATAGCCCCTTA[R->A/G]CCAGTTGTATATTA
2	TGTGCACAC[R->A/G]TTAGGC
3	AATGTATTCT[M->A/C]TCTCTCTTT
4	AAGGATGACTA[Y->C/T]AGACATTAAATAATC

Table 2. Affection Status of Drexel University AA AD Cohort

Diagnosis	#
Early Onset AD	1
Late Onset AD	34
Mild Cognitive Impairment	4
Mixed	13
Vascular Dementia	4
Control	53
Unknown	2
TOTAL	111

Research Project 11: Project Title and Purpose

Suppression of Monocyte Migration by Inducible CCR2 Silencing - The purpose of this work is to develop a new method to intervene in the progression of neurologic disease that often occurs in HIV-1 infected individuals. We will investigate a method designed to reduce the ability of HIV-1 infected immune cells to migrate into the brain. This migration is enhanced by signals released from brain-resident infected cells in a positive feedback loop that we will disrupt using a strategy based on RNA interference. Certain receptors that are present on the surface of immune cells, and that allow these cells to respond to the migratory signals, will be down-regulated specifically in HIV-1 infected cells. If successful, this will lead to therapies designed to reduce the overall inflammatory immune response to infection in the brain and help to curb the progression of neurologic disorders.

Anticipated Duration of Project

1/1/2010 - 12/31/2011

Project Overview

HIV-1 associated dementia (HAD) and a more subtle condition called minor cognitive motor disorder (MCMD) are neurological disorders that develop in a high percentage of HIV-1 patients and correlate with a worse overall outcome. Although control of viral load using anti-retroviral therapies (ART) has reduced the severity of these neurological diseases, longer patient survival times have increased their prevalence. Further, the failure of existing ART to cross the blood brain barrier (BBB) limits its efficacy in treating HIV-1 infection in the brain. In the experiments of this project, we will address these issues by using a lentiviral vector, that we developed in previous work, that expresses a microRNA (miRNA) designed to suppress the expression of a cytokine receptor (CCR2). The vector will be used to tranduce monocytes, where the CCR2 receptor plays a central role in monocyte migration across the BBB in response to MCP-1 (CCL2), a cytokine that is induced by exposure of astrocytes to the viral protein Tat. The CCR2-miRNA is expressed from a Tat-inducible RNA polymerase II promoter and thus silencing is limited to HIV-1 infected cells, protecting the functional integrity of uninfected monocytes. We expect that this strategy will help to interrupt a positive feedback loop where

infected monocytes would otherwise be attracted into the brain by MCP-1 that, in turn, was induced by Tat released from brain-resident infected cells. In the current phase of the project, we will test whether transduction with our lentiviral vector affects aspects of monocytes physiology and whether sufficient miCCR2 can be induced by HIV-1 infection to suppress migration of transduced monocytes. We recognize that additional toxic factors are released in the brain of an infected patient and contribute to neuronal damage. The work of this project is meant to be a proof-of-principle study that focuses on a major regulatory circuit, but where additional elements can be added to our highly adaptable silencing vectors in the future.

Principal Investigator

Laura F. Steel, PhD
Assistant Professor
Drexel University College of Medicine
245 N 15th St
MS 1013A
Philadelphia, PA 19102

Other Participating Researchers

Michele A. Kutzler, PhD, Jeffrey M. Jacobson, MD - employed by Drexel University College of Medicine

Expected Research Outcomes and Benefits

This work can provide the basis for a novel approach to HIV-1 therapy that addresses both viral replication and disruptions of cellular signaling that are responsible for much of the pathogenesis of this disease. While there has been a degree of success in the treatment of HIV-1 with current anti-retroviral therapies (ART), these treatments remain problematic in terms of cost, unwanted side effects, patient compliance, and long-term efficacy. In addition, the neurological disorders associated with HIV-1 infection have been particularly difficult to treat since most medications will not cross the blood-brain barrier. The work of this project explores the idea that cellular signaling pathways that affect disease progression can be specifically disrupted in HIV-1 infected cells. By targeting cellular pathways instead of viral gene products, we expect to reduce the problem of escape by this highly mutable virus. However, our strategy also preserves the functionality of important cells of the immune system that are not infected by HIV-1. We expect that this work will help to identify cellular regulatory networks that play key roles in neurological disease progression as well as to develop new strategies to disrupt these networks in a therapeutically significant way.

Summary of Research Completed

The goal of this project has been to test whether expression of the MCP-1 receptor, CCR2, on the surface of primary human monocytes, can be knocked down by transduction of cells with lentiviral vectors that express microRNAs (miRNAs) designed to target the CCR2 mRNA. Further, we planned to test whether the miRNAs could be expressed in HIV-1 infected cells from

a Tat-inducible promoter, the CK-TAR promoter, that we described in earlier work. In the long-term, we hoped to be able to suppress the MCP-1 directed migration of HIV-1 infected monocytes into the central nervous system, without affecting the function of uninfected monocytes.

1. Transduction of primary human monocytes with a lentiviral vector that expresses miRNAs that target CCR2 mRNA.

In a previous report on a related project, we have described the construction of a lentiviral vector, pLEX-GFP, that can be used for the expression of miRNAs. This lentivector carries a bicistronic gene encoding turboGFP (tGFP) and puromycin resistance, driven by a CMV promoter and separated by an IRES element, so that transduction can be followed (green cells) and integrants can be selected (puromycin resistance). The pLEX-GFP vector was used to generate VSV-G pseudotyped viruses that expresses two different CCR2-miRNAs (miCCR2-D/E) under the control of a CMV promoter (for constitutive expression) or the CK-TAR promoter (for Tat-inducible expression). The miCCR2-D and miCCR2-E miRNAs had been tested separately, using plasmid expression vectors, and shown to provide moderate reductions of CCR2 mRNA in HEK-293T cells co-transfected with the silencing plasmids and a CCR2 expression plasmid. The lentiviral vector was then constructed where both miRNAs are processed from a single transcript, using a design developed in our lab.

CCR2 is a receptor that is expressed on the surface on human monocytes (as shown by FACS analysis in a previous report), and we attempted to downregulate this expression using the pseudotyped lentiviruses carrying miCCR2-D/E expression cassettes. The extremely low efficiency of transduction of the primary monocytes with our vectors (and additional control vectors) together with the modest silencing we were able to achieve with miCCR2-D/E, made it impractical to continue with these experiments. Nevertheless, we were anxious to move forward to investigate the possibility of using the Tat-inducible CK-TAR promoter to express miRNAs with anti-viral properties so that both viral and cellular transcripts might be targeted, with minimal potential of doing harm in uninfected cells. (Solving the monocyte transduction problem will become part of a longer term project.) Our use of the CK-TAR promoter in lentiviral vectors to suppress HIV-1 replication is described in Section 2, below.

2. Induction of anti-viral miGag expression in virus infected cells.

We have previously tested the antiviral activity of miGag, an miRNA that targets HIV-1 transcripts in a region that encodes Gag, and found it to be a potent suppressor of viral replication when expressed from plasmids that are delivered at high copy number to cells by transient transfection. We sought to test the efficacy of this miRNA in the more clinically relevant context of delivery by lentivectors and stable incorporation of far smaller copy numbers (approximately one) into the cellular genome. Further, our initial experiments had used co-transfection with HIV-1 Tat expression plasmids to demonstrate the Tat inducibility of the CK-TAR promoter and we wanted to extend those results to ask whether enough Tat is produced in virus infected cells to induce expression of miGag to levels that can suppress viral replication. Lentiviral vectors that express miGag have been constructed, with expression driven by either the CMV or CK-TAR promoter. These lentivectors are in the same background (pLEX-GFP)

described above and so express both tGFP and puromycin resistance. HeLa-CD4 cells are stably transfected to express the CD4 cell surface marker, and they are infectable by HIV-1. We have transduced HeLa-CD4 cells with CMV-miGag, CK-TAR-miGag, and CMV-miFlu (control) lentiviral vectors and selected for integrants by growth in puromycin. These cells were then infected with HIV-1 (strain LAI) and virus replication was assayed two days post-infection. The results are shown in Figure 1 and demonstrate that transduction with the CMV-miGag lentivector suppresses viral replication as compared to the irrelevant CMV-miFlu lentivector, as expected. The CK-TAR-miGag lentivector also suppresses viral replication. Since we have shown previously that the CK-TAR promoter has very low basal activity in the absence of Tat induction, these results support the interpretation that Tat produced in infected cells is sufficient to induce expression of miGag. Additional experiments to verify this conclusion, and to measure the copy number of integrated vector, are underway.

3. Suppression of silencing by miRNAs in HIV-1 infected cells.

There have been several reports that HIV-1 gene products can globally suppress RNA silencing in infected cells and that this acts as a viral countermeasure against cellular RNAi-mediated defense mechanisms. These claims have been controversial, but understanding the interplay between the virus and RNAi pathways is clearly important when devising anti-viral therapies based on silencing. Therefore, we examined whether the viral Tat protein is truly a suppressor of RNAi and whether there is any indication of global suppression of RNAi pathways in the presence of replicating virus.

Using several measures of silencing by both exogenous and endogenous miRNAs, we have shown that reported suppressor of RNA silencing (SRS) activity of Tat is due to its activity as a transcriptional transactivator, and not SRS activity. In the experiment shown in Figure 2, HeLa-P4R5 cells were co-transfected with pdsEGFP and a plasmid encoding miEGFP, in the presence or absence of a Tat expression plasmid, pwtTat. The suppression of EGFP expression by miEGFP appears to be suppressed by co-expression of wild type Tat (lanes 1-4). However, when a transcriptionally inactive Tat mutant (K41A-Tat) was co-expressed, the apparent SRS activity disappeared (lanes 5 and 6). Further, when cells were transfected with pwtTat in the absence of the silencing plasmid, it was evident that Tat alone can substantially increase the expression of the EGFP reporter (lanes 7 and 8) although expression of the mutant K41A Tat did not affect EGFP levels (lanes 9 and 10). These results show a direct relationship between the transcriptional activity of Tat and its ability to up-regulate EGFP reporter expression, in a manner independent of silencing.

To test the effects of Tat on silencing mediated by endogenous cellular miRNAs, we used a dual luciferase reporter plasmid, psiCHECK-2, where target sequence for an miRNA is inserted into the 3'-untranslated region of a Renilla luciferase gene and firefly luciferase is expressed from an independent gene on the same plasmid to serve as a transfection efficiency control. Silencing of Renilla luciferase by miRNAs targeting the inserted sequence is reported as a reduction in the ratio of Renilla to firefly luciferase activity. Results shown in Figure 3 indicated that transfection of cells (HeLa or HeLa-P4R5) with a psiCHECK-2 reporter carrying target sequence for miR-16 (psiCH2-16T) gave no indication of reduced silencing in the presence of co-transfected Tat, again arguing against an SRS activity for Tat.

Additional mechanisms of HIV-1 suppression of silencing have been proposed, including the potential sequestration of TRBP (an essential co-factor of Dicer in miRNA processing) by its binding to the TAR element of HIV-1 transcripts. Therefore, we investigated whether products of HIV-1 replication, in addition to Tat, could suppress RNA silencing. The target site in psiCH2-16T is perfectly complementary to miR-16 and so we also constructed a second plasmid, psiCH2-cycE1, that contains the imperfectly matched sequence found in the validated miR-16 target, cycE1 mRNA to more closely mimic natural silencing. In addition, we constructed a reporter where the miR-16 target sites were mutated by site-directed mutagenesis, to act as a control. Silencing of the Renilla luciferase activity from these reporter plasmids was tested in both HEK-293T cells and in Jurkat T-cells by co-transfection with the HIV-1 infectious molecular clone, pLAI. Results shown in Figure 4 indicated that there was no reduction in the silencing capacity of endogenous miR-16 in the presence of replicating virus in either HEK-293T cells or in Jurkat cells. The results of these and additional experiments demonstrate that HIV-1 does not act to globally suppress cellular silencing. These experiments are more fully described in a publication that resulted from this work:

Sanghvi, V.R. and Steel, L.F. 2011. A re-examination of global suppression of RNA interference by HIV-1. PLoS One 6(2), e17246.

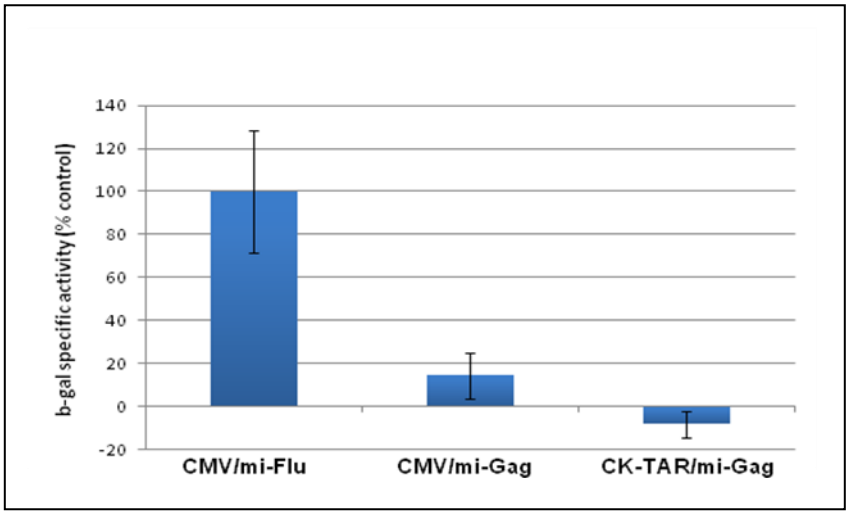

Figure 1. Suppression of viral replication by Tat-induced expression of miGag in virus infected cells. Stable HeLa-CD4 transductants were prepared from cells transduced with CMV-miFlu, CMV-miGag, and CK-TAR-miGag lentivectors. Cells were infected with HIV-1 (LAI) virus and extensively washed. Two days post-infection, supernatant was collected and viral replication was quantified by an infectivity assay where HeLa-P4R5 indicator cells were treated with equal amounts of supernatant from each of the infected cell samples. Infectious virus was measured by the induction of β-galactosidase in the indicator cells. Results are presented as percent of activity from the control CMV/miFlu cells and error bars show the standard deviation from 8 experimental replicates.

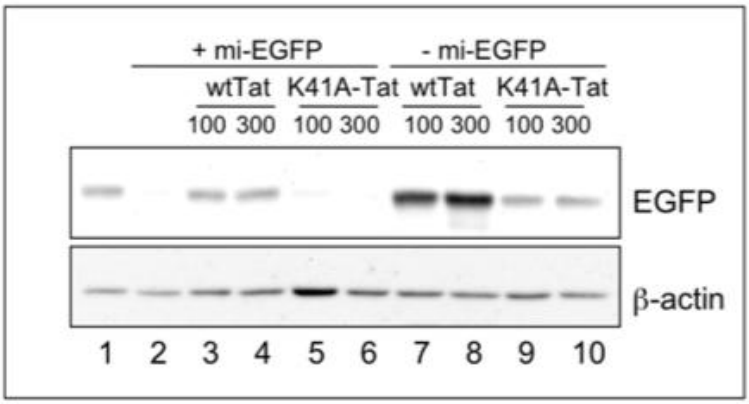

Figure 2. Apparent SRS activity of HIV-1 Tat protein is due to transcriptional activation of reporter expression. Immunoblot analysis of EGFP expression in the presence or absence of a silencing plasmid (mi-EGPP) and wt-Tat or K41A-Tat plasmids, as indicated. Detection of β-actin serves as a loading control.

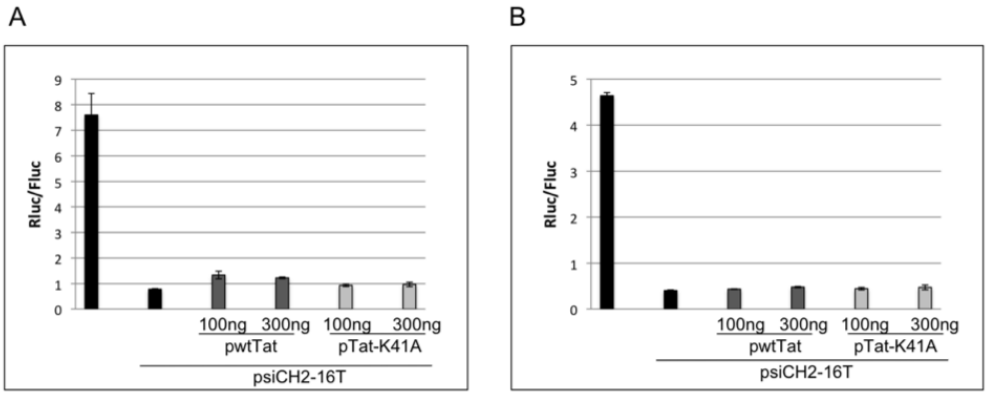

Figure 3. Tat overexpresssion does not reduce silencing mediated by endogenous miR-16. A) HeLa cells, B) HeLa-P4R5 cells.

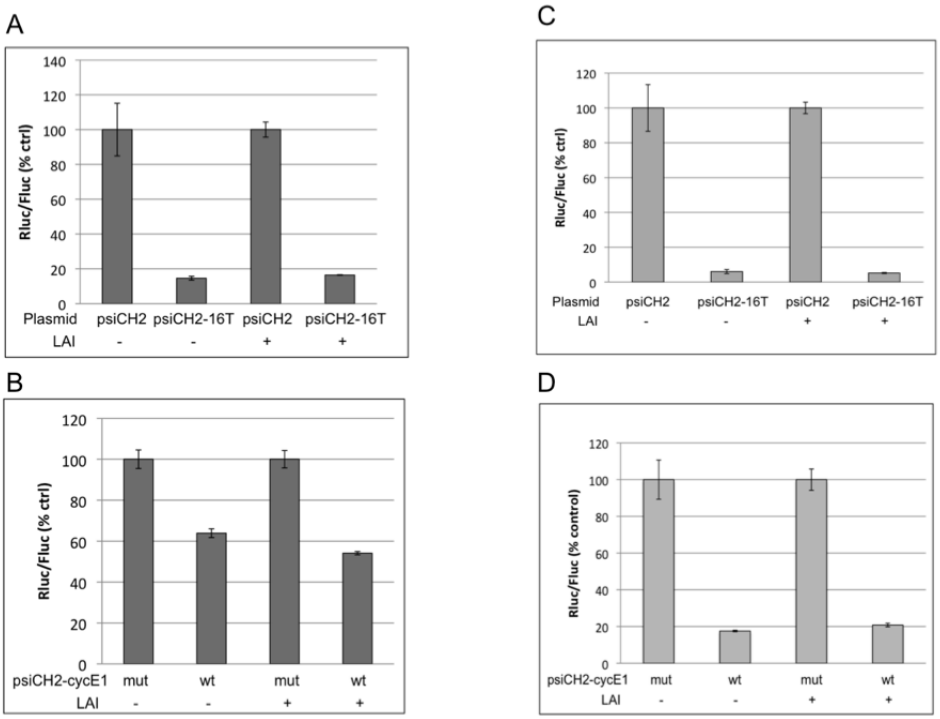

Figure 4. Silencing efficacy of endogenous miR-16 is not affected by the presence of replicating virus. A) 293T cells were transfected with a reporter plasmid, either psiCH2 (empty plasmid) or psiCH2-16T, together with or without pLAI, as indicated. Cell lysates were prepared and luciferase activity was assayed 2d post-transfection. Data are normalized to the respective psiCH2 control. B) 293T cells were transfected with either psiCH2-wtE1 or psiCH2-mutE1, in the presence or absence of pLAI, as indicated. Cells lysates were analyzed for luciferase activity as in (A). Data are normalized to the respective psiCH2-E1 control. C) Jurkat cells were transfected and analyzed for the efficacy of miR-16 silencing as in (A). D) Jurkat cells were transfected and analyzed as in (B). Error bars represent standard deviation from 4 replicates.